PIEZOELECTRIC VIBRATION ENERGY HARVESTER
WITH MOVABLE TIP MASS

by
Cevat Volkan Karadağ

Submitted to Graduate School of Natural and Applied Sciences
in Partial Fulfillment of the Requirements
for the Degree of Master of Science in
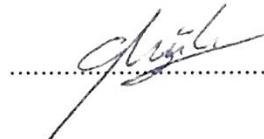Mechanical Engineering

Yeditepe University
2016

PIEZOELECTRIC VIBRATION ENERGY HARVESTER

WITH MOVABLE TIP MASS

APPROVED BY:

Assist. Prof. Dr. Nezih Topaloğlu

(Thesis Supervisor)

Assist. Prof. Dr. Gürhan Küçük

Assist. Prof. Dr. Süleyman Serdar Yörük

DATE OF APPROVAL: ..../..../2016

ACKNOWLEDGEMENTS

ABSTRACT

PIEZOELECTRIC VIBRATION ENERGY HARVESTER
WITH MOVABLE TIP MASS

This thesis presents a novel smart vibration energy harvester that is able to automatically adjust its natural frequency. The proposed harvester preserves the electrical power generating element in a resonance with ambient vibration in order to maximize power yield. The structure consists of two piezoelectric cantilever beams, a miniature piezomotor with a movable mass connected to one of the beams, a control unit and electronics. The piezomotor does not require energy to fix its movable mass as a result of its self-locking feature. At each predefined interval, the control unit performs voltage comparisons where each level crossing provides timings to calculate the phase difference between two beams. When necessary, it actuates the piezomotor to move its mass in the appropriate direction. After completing its tasks, the control unit switches to the power-saving sleep mode. It is shown that the proposed tuning algorithm successfully increases the fractional bandwidth of the harvester from 4% to 10%. A piezomotor having longer range of motion will improve this value. The system is able to deliver 66.8% of the total harvested power into usable electrical power while the piezomotor actuation uses only 3.6% of the harvested power. The presented efficient, auto-tunable and self-sufficient harvester is built using off-the shelf components and it can be easily modified for wide range of applications.

ÖZET

UCUNA HAREKETLİ KÜTLE BAĞLI TİTREŞİM BAZLI PİEZOELEKTRİK ENERJİ TOPLAYICISI

Bu tez, doğal frekansını otomatik olarak ayarlayan yenilikçi bir titreşim bazlı enerji toplayıcısı sunar. Önerilen toplayıcı, elektrik üreten elemanı ortam titreşimi ile rezonans durumunda tutarak azami güç verimi sağlar. Yapı, iki adet piezoelektrik konsol kiriş, kirişlerinden birinin ucuna hareketli kütle bağlı bir minyatür piezomotor, kontrol ünitesi ve devre elemanlarından oluşur. Sabit konumda özkilitlenme özelliği sayesinde durağan halde enerji harcamaz. Önceden belirlenmiş aralıklarda, kontrol ünitesi, iki kirişin potansiyel farklarının seviye geçiş sürelerinin karşılaştırılması yoluyla iki kiriş arasındaki faz açısını hesaplar. Gerekli olduğu takdirde pizeomotor kütleyi uygun yönde harekete geçirir. İşlerini bitirdikten sonra, kontrol ünitesi enerji tasarruflu uyku moduna girer. Önerilen algoritmayla fraksiyonel bant genişliğinin %4'ten %10'a arttığı gösterilmiştir. Daha uzun hareket menziline sahip bir piezomotor kullanılması durumunda bu değer daha da arttırılabilir. Piezomotor hareketinin toplanılan gücün sadece %3,6'sını kullanmasının yanısıra, sistem üretilen enerjinin %66,8'ini kullanılabilir durumda korur. Sunulan etkili toplayıcı, kendini otomatik ayarlayan ve kendi kendine yeterli, kolayca elde edilebilen parçalardan yapılabilir ve farklı uygulamalarda kullanıma uygundur.

TABLE OF CONTENTS

LIST OF FIGURES

LIST OF TABLES

LIST OF SYMBOLS/ABBREVIATIONS

c_i	Effective Damping Coefficient
k_i	Effective Spring Constant
m	Effective Tip Mass
t	Time
T_i	Level Crossing Time
ΔT_i	Difference of Level Crossing Time
υ	Sampled Time Difference Data
Z_i	Tip to based displacement
θ_i	Phase of a beam
ξ_i	Effective Damping Ratio
ω	Frequency of excitation
ω_{ni}	Natural frequency of beam
CPU	Command Processing Unit
DAQ	Data Acquisition
MCU	Microcontroller unit
PVDF	Piezoelectric polyvinylidine fluoride
RMS	Root-Mean-Square
VEH	Vibro energy harvester

1. INTRODUCTION

The advances in low-power electronics give rise to popularity of energy harvesting systems for powering wireless sensors networks, instead of electromechanical batteries. Among various ambient energy sources, mechanical vibrations own the advantage of being abundant in moving/oscillating systems, especially when solar energy is absent [1]. Vibration energy harvesters utilize these mechanical vibrations to produce electrical power. Most vibration energy harvesters consist of a sprung mass attached to a mechanical spring, with a mechanical-to-electrical transduction mechanism. The main challenge of a vibration energy harvester (VEH) is that the frequency of ambient vibration fluctuates significantly in many applications, whereas the natural frequency of the harvester is fixed. Therefore, the harvester is usually at out-of-resonance condition, in which the harvested power is significantly low, compared to the resonance case [2-4], see Figure 1.1, and details at section 3.1.
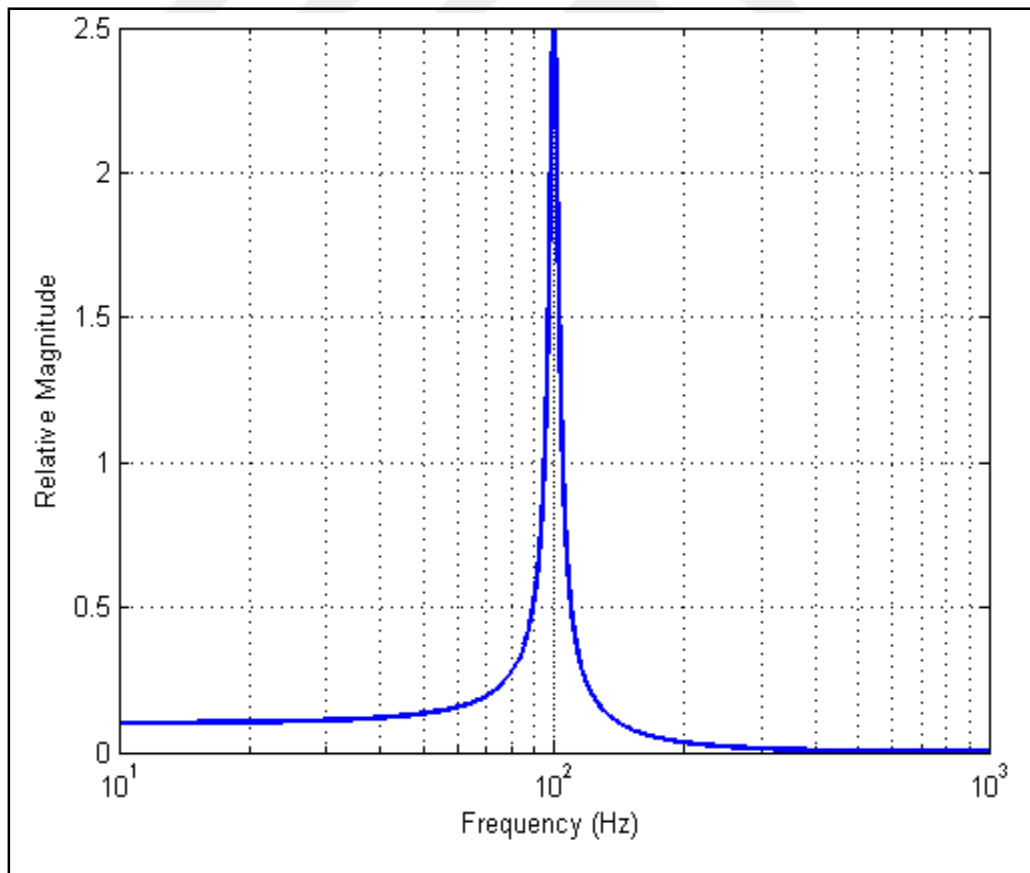
Figure 1.1. The analytic frequency response of a second order mechanical spring-mass-dampener system ($\xi = 0.02$)

1.1.   LITERATURE REVIEW

To avoid the aforementioned problem, various solutions have been proposed so far. A general overview on the efforts of developing wideband VEHs can be found in [5]. A simple solution proposed was to have a group of piezoelectric cantilever beam VEHs having different resonance frequencies [6]. The idea is to obtain a wideband response by having at least one beam at resonance. However, the power harvested by the beams in out-of-resonance condition is dramatically low. Therefore, the overall power density of the harvester is not satisfactory. Previous studies have shown that nonlinear (softening or hardening) springs can widen the bandwidth of a VEH [7-14]. A mechanical frequency up-conversion method for harvesting energy is also a non-linear method which is designed to harvest energy from low frequency of ambient vibration [15] where one of the two existing beams usually has a proof mass and the other serves electricity generating purposes in high frequency of oscillation. In this method, the proof mass can oscillate in a range of low frequencies, such as 1 to 10, see Figure 1.2.
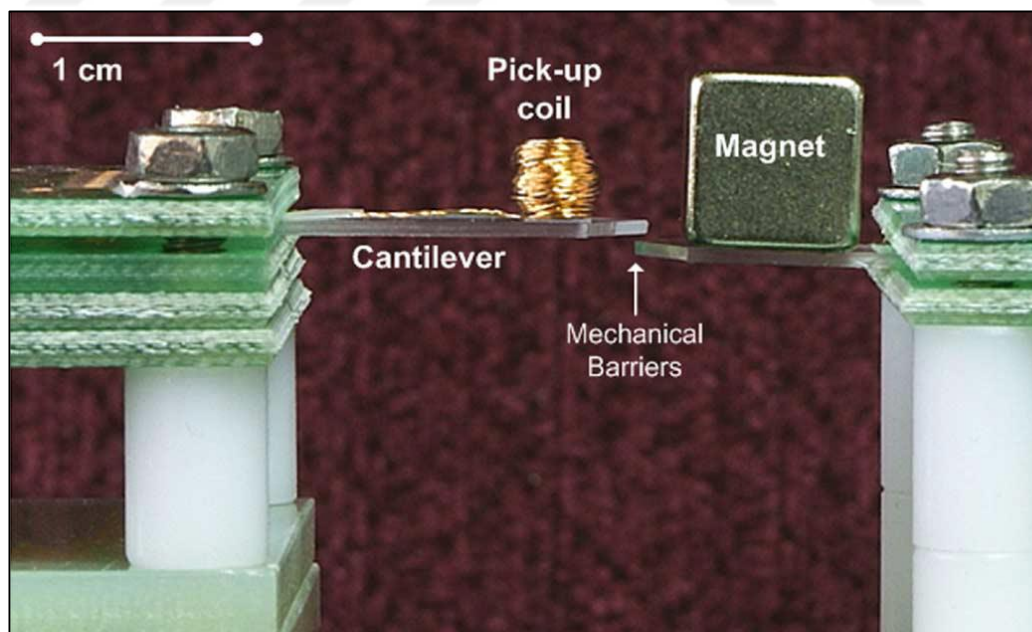
Figure 1.2. Frequency Up-conversion Method VEH Prototype [15]

In addition, it was shown that adding nonlinearity in the energy harvesting/damping component of a VEH can result in increased bandwidth as well [16]. However, some

limitations of these techniques are reported [5]. The performance of tuning depends highly on ambient vibration amplitude. At low amplitudes, the non-linear effect is severely reduced. In addition, a high hysteresis in response is observed and the system response to random excitations exhibit chaotic behavior [5, 10].

Other than the passive approaches explained above, approaches based on actively tuning the harvester natural frequency have also been studied. The natural frequency tuning approaches can be classified as manual and automatic tuning. In manual tuning, the natural frequency of the harvester is tailored manually prior to the installation of the harvester. Mansour et al used a PVDF generator beam with a tip magnet, and a fixed magnet set close to the tip magnet by a screw with locking nuts [17]. By using the screw, the distance between the magnets can be arranged so that the effective stiffness of the beam can be tuned, see Figure 1.3.
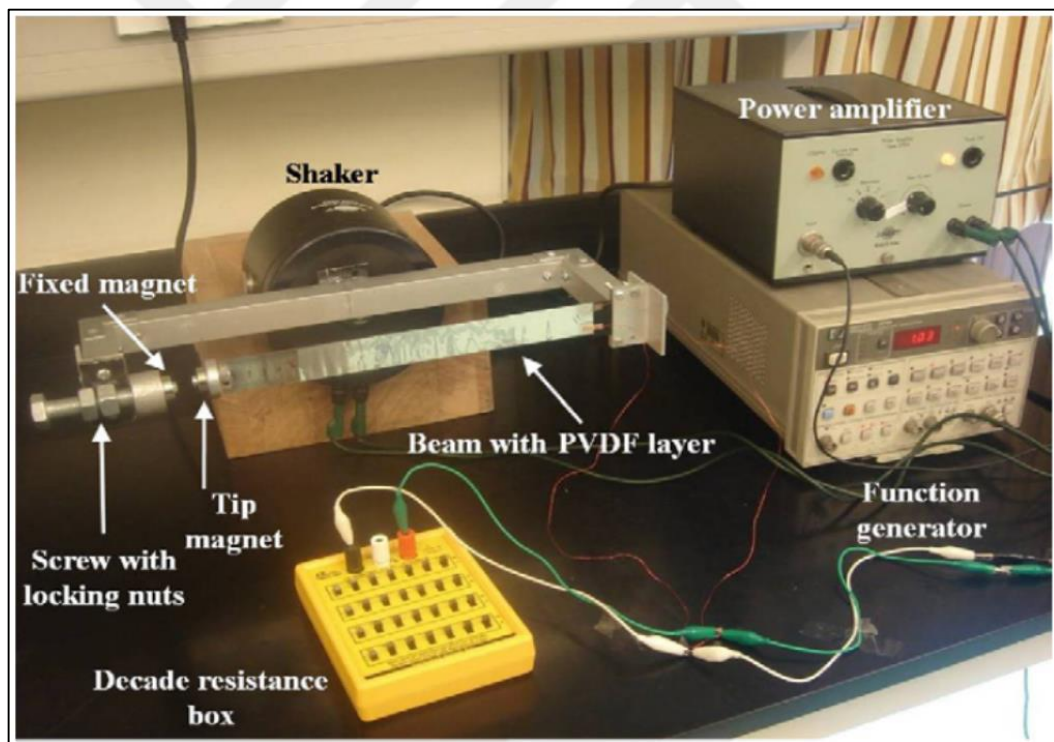
Figure 1.3. Manual Tuning Experimental Setup [17]

In another approach by Turkyilmaz et al, a magnetic proof mass is fixed to a flexiglass frame by four rubber springs [18]. The tension on the rubber springs can be manually adjusted, thus the effective stiffness of the harvester can be tuned. Manual tuning, however, are not

practical in many applications, especially when the ambient vibration frequency varies frequently and when the harvester is not easily accessible, see Figure 1.4.
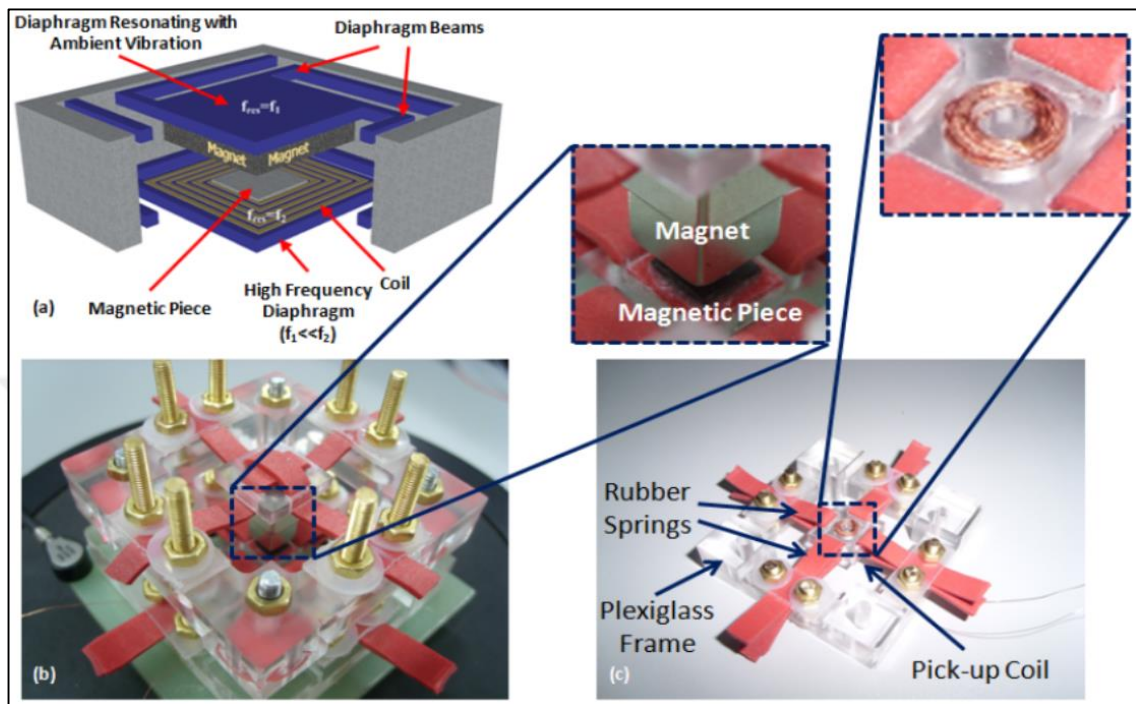
Figure 1.4. (a) The generator structure, (b) the whole system, (c) the lower diaphragm [18]

Automatic tuning of the harvester natural frequency has the theoretical advantage of being in resonance without any user interruption. On the other hand, this technique requires an actuator, and a controller that uses the actuator to actively tune the natural frequency. This smart system will also consume electrical power, which poses strict requirements on the power budget. As an example of automatically-tuned systems, Huang et al used a cantilever beam VEH with a moving support, which is connected to a stepper motor [19], see Figure 1.5.
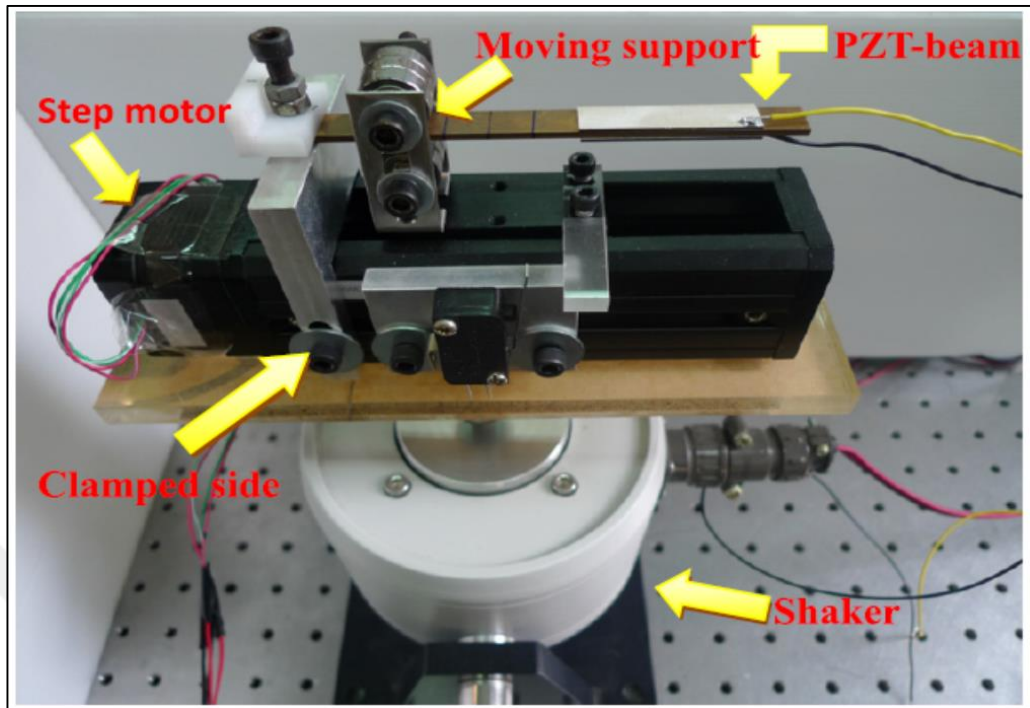
Figure 1.5. Map-Tuning Piezoelectric VEH [19]

In this study, the cantilever beam length and thus its natural frequency is tuned by moving the beam support position with the stepper motor. A look-up table is implemented for effective tuning. The experiments revealed that wideband response is obtained; however, the size of the system makes it impractical to use in many applications. In addition, the system is not stand-alone, and is not self-sufficient due to high energy consumption of the stepper motor, see Figure 1.5.

Recently, a compact prototype of a smart, frequency tunable VEH was developed by Eichhorn et al [20]. Their device includes a piezoelectric generator beam for energy harvesting purposes and a piezoelectric actuator beam to create axial stress on the generator beam. The actuator beam alters the generator beam's stiffness to tune its natural frequency. They implemented a look-up table on a low-power microcontroller for frequency tuning, and used a commercial accelerometer to update the look-up table periodically. Although self-sufficient operation was successfully demonstrated at some fixed ambient frequency values, the piezoactuator beam requires energy to sustain its axial strain level. This energy requirement is due to the high voltage requirement of the piezoactuator, which needs to be supplied by a step-up converter, see Figure 1.6.
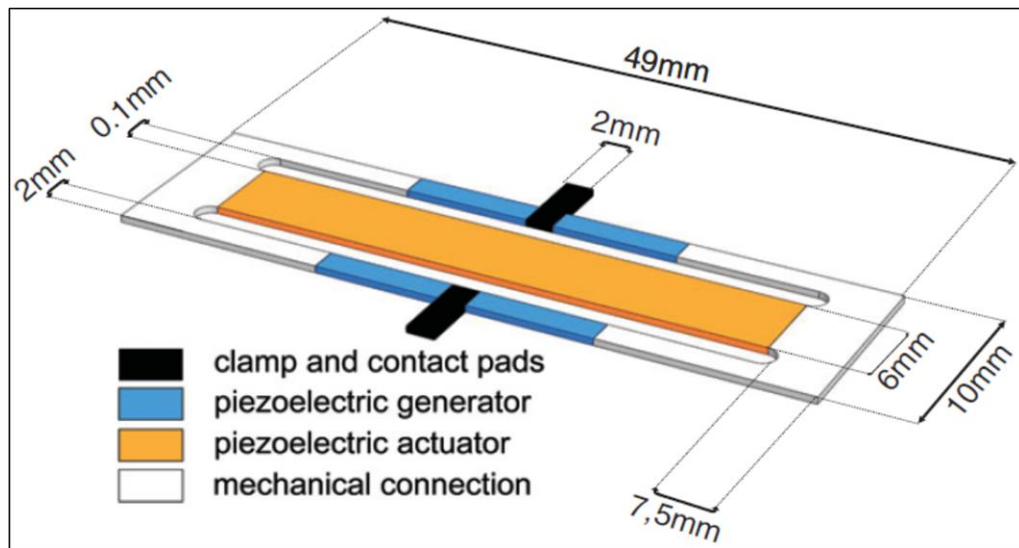
Figure 1.6. Three-dimensional scheme of the generator design [20]

At high supply voltages, the leakage current of the piezoactuator rises, which results in additional energy loss. In addition, the piezoactuator requires significant amount of energy when the natural frequency needs to be altered, as well. Therefore, the system is unable to exhibit self-sufficient operation and requires external source of power, at varying frequency conditions. The accelerometer used for look-up table updating also requires a considerable amount of energy, see Figure 1.7.
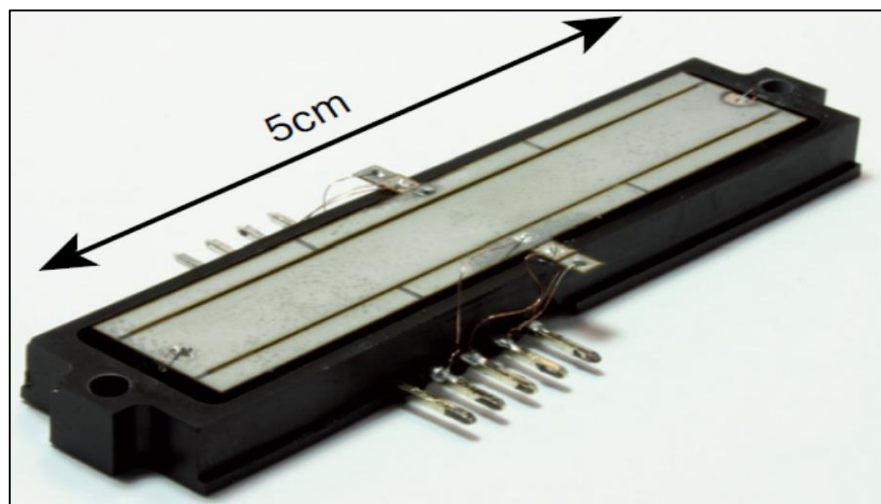
Figure 1.7. Photograph of the frequency-tunable piezoelectric
energy-harvesting device [20]

1.2.   OBJECTIVES

The objective of this thesis is to produce sufficient amount of electrical energy from environment to run microcontroller devices or wireless sensor nodes, etc. by utilizing the vibrating sources in the case of frequency sweep.

1.3.   OUTLINE OF THE THESIS

The device structure is described and the piezomotor features are given in Section 2. The electrical and mechanical properties of piezo coupled beam and PiezoWave® actuator are studied. Initial device structure is mentioned, followed by the second which is the proposed current structure is explained. In Section 3, the theory of the tuning algorithm is elaborated with prompt sensitivity analysis. The implementation of the proposed tuning algorithm in a low-power microcontroller is prepared and simplification of the algorithm is consolidated into the device the power harvesting circuitry is given in section 4. The experimental results, including the algorithm performance and tuning in various conditions and a power distribution analysis are provided in section 5. Finally, conclusions are drawn in section 6.

2. DEVICE STRUCTURE

In this thesis, we present a smart and self-sufficient VEH with self-adjustable natural frequency. The main idea is to use a small linear actuator, fixed on the tip of a piezo-coupled generator beam (Mide^{TM}). The linear actuator tunes the natural frequency of the beam by moving a connected tip mass back and forth in the axial direction. As the linear actuator, a tiny piezomotor is used, see Figure 2.1.
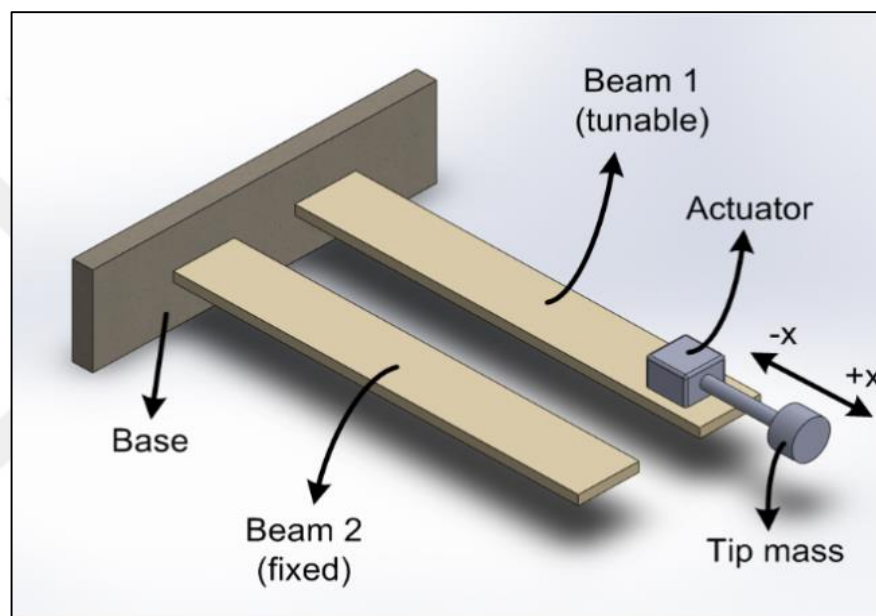
Figure 2.1. Proposed device structure of the concept design

Piezomotor has advantages of having fast response, low power consumption and small dimensions. More importantly, unlike a piezoelectric actuator beam, the piezomotor is self-locking, therefore it can easily fix the tip mass without consuming any energy. This way, the overall power consumption at a constant ambient frequency can be reduced to very low levels. To make the decision on which direction to move the tip mass, a second piezo-coupled beam is used and a phase-detection based decision algorithm is applied. Using a second beam instead of a commercial accelerometer decreases the overall energy demand. The system is able to tune its natural frequency and stays in resonance in a self-sufficient manner, without being affected by the nonlinearities in the system. In this chapter these components are described first and details of assembling these components is discussed later.

2.1. PIEZO COUPLED BEAM

A commercially available energy harvester is selected as a suitable constituent electrical generator part which is Mide^{TM} Volture BL-21, a simple energy harvester that takes advantage of two piezo patches on each sides, see Figure 2.2.
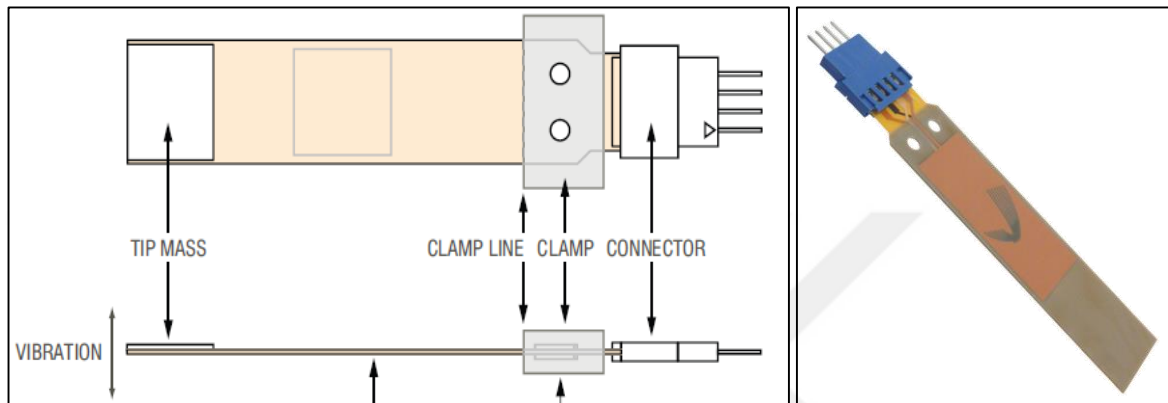
Figure 2.2. Mide™ Energy Harvester

The dynamic behavior of the piezo coupled energy harvester beam is examined by frequency sweep without a tip mass. The open circuit potential difference at the terminal of one piezo patch is recorded in order to plot frequency response of the harvester assuming the deflection is directly proportional to the terminal voltage, see Figure 2.3.
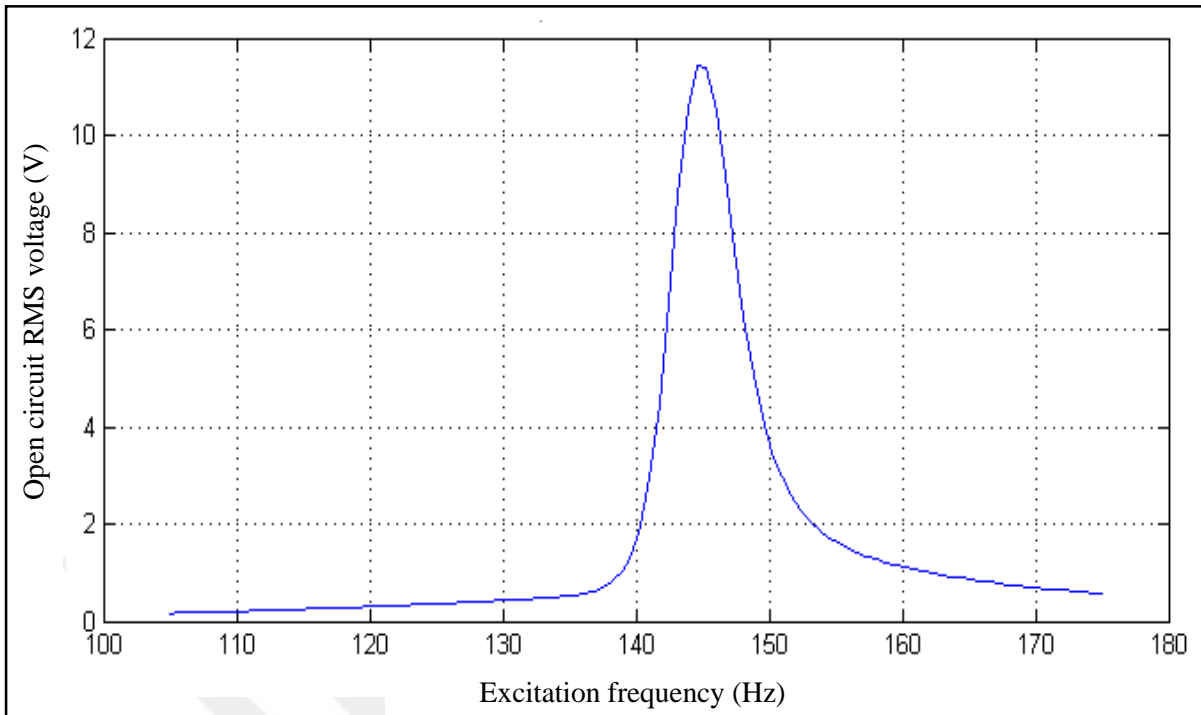
Figure 2.3. Frequency response of Mide™ bl-21

In order to conduct a simple electrical model of the generator different electrical loads are placed and the terminal voltages are monitored. The heat dissipation of the load is maximized between 40-50Kohm of load resistor when resonance occurs. However, this value is effected by the frequency of operation. Figure 1.2 shows the energy surface of one patch with a roughly 0.3gram of tip mass, see Figure 2.4.
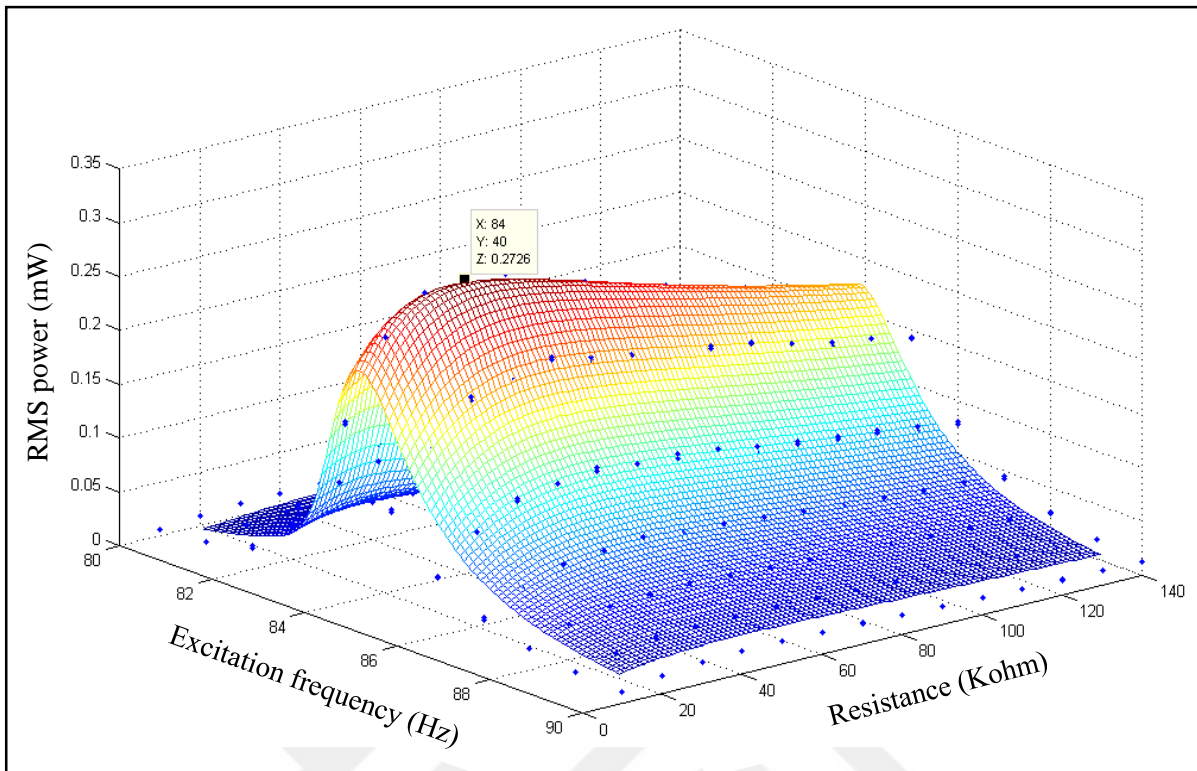
Figure 2.4. Heat dissipation of the resistor load to different frequency of excitation

The storage test is done with the help of a simple capacitor charging circuit. A simple rectification unit is placed directly between the terminals of the generator beam and the storage capacitor seen on the Figure 2.5. The change of the potential difference of the capacitor voltage indicates the net power delivered to the capacitor by the help of the constitutive capacitor expression, similar to the one on the section 5.3. The effective resistive load of the capacitor can be also estimated via the capacitor voltage under a constant mechanical excitation by using Ohm's Law, and the experiment results for placing roughly 1 gram of tip mass on one Mide™ bl-21 is shown on Figure 2.6 under 50 Hz of excitation.
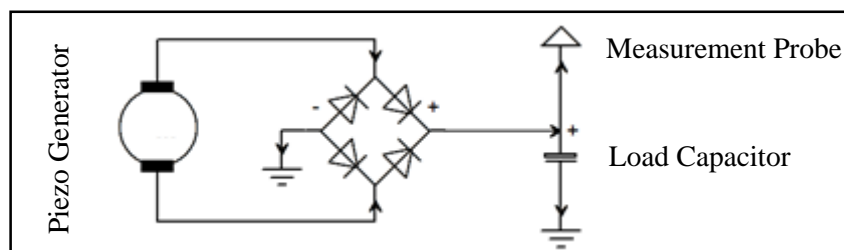
Figure 2.5. Simple Capacitor Charging Circuit
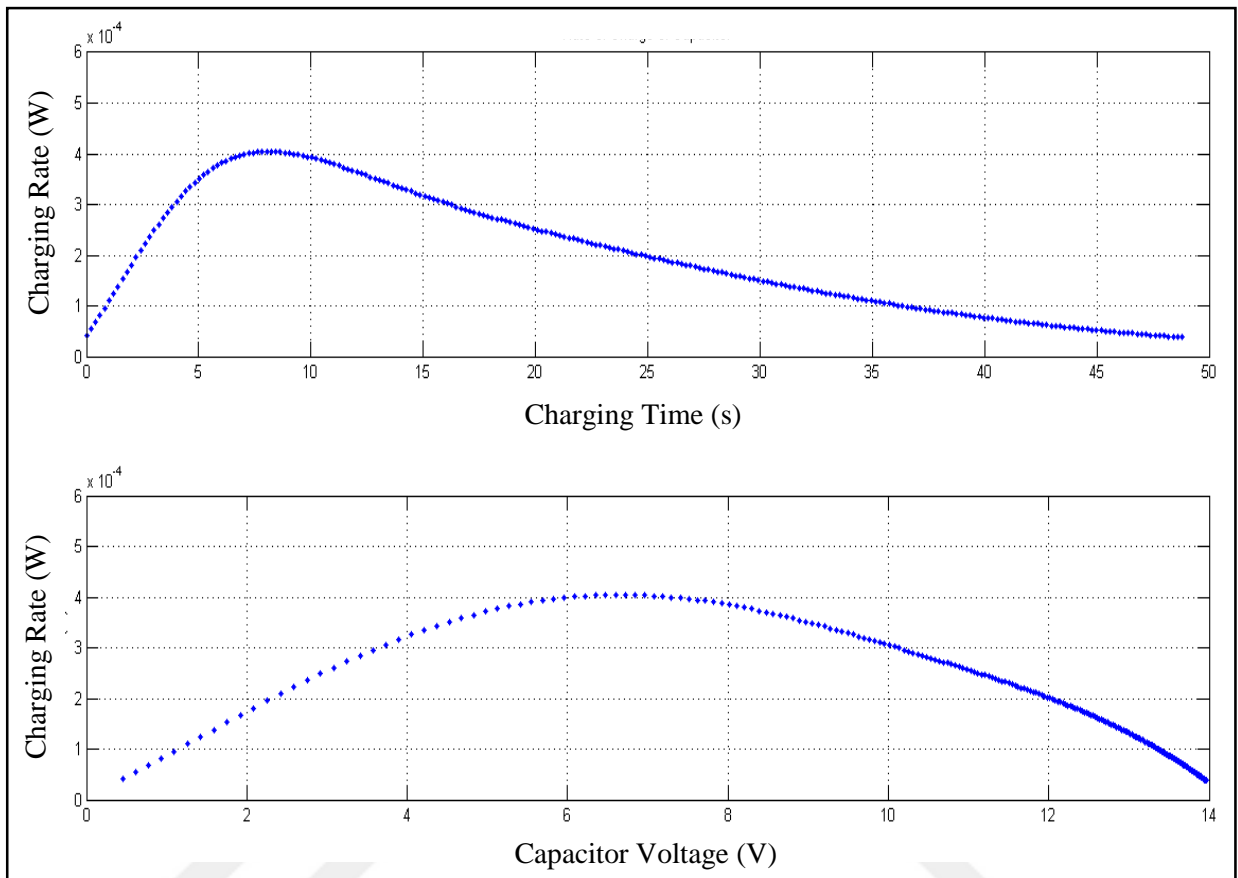
Figure 2.6. Capacitor Charging, Power vs. Time (Upper), Power vs. Voltage (Lower)

The estimated effective load is found between 40-50Kohm for different constant frequencies of excitation. The connection of two piezo patches gives two advantages applications; the one lower the optimum load by two times and the second is the multiplication of the terminal voltage by two. Some applications may require higher voltage and halving optimum load by gives two times more current. In both of available options helps to obtain two times more power than a single patch.

2.2.   PIEZO ACTUATOR
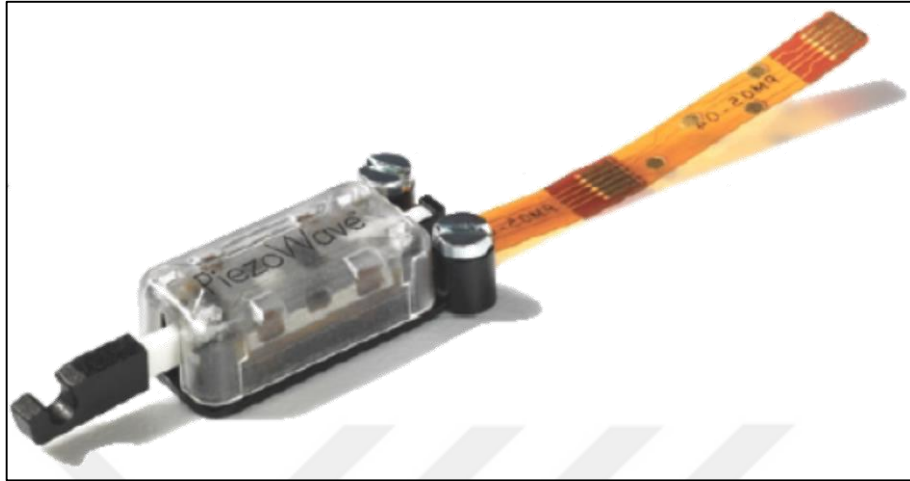
Figure 2.7. Picture of PiezoWave® Motor [22]

The proposed actuator is a piezomotor, see Figure 2.7. PiezoWave® motor is a friction-based motor with a small drive force of 0.5N, i.e. the motor should overcome friction to move the tip mass. This seems to be a disadvantage, however it gives the motor no backlash with a self-locking feature (0.3 N), which means no additional power is required to keep the tip mass position fixed. The importance of keeping the position fixed without using any source of power becomes significant when there is no change in the frequency of the ambient vibration, and therefore overall energy requirement to tune the proposed self-tunable VEH can be reduced significantly by using a self-locking featured actuator.

The use of a piezomotor has also the advantages of scalability. The selected piezomotor is very small (longest dimension 14 mm) and lightweight (0.6 grams). The total tip mass displacement range is 8 mm. Electricity consumption is 35 mA at 3.3V with a speeds of 100 mm/s. Additional dimensions and power consumption data of the piezomotor is given in [22]. Energy consumption this type of actuator is deterministic since it consumes same amount of power regardless of the load on it, the constant energy consumption helps to estimate the energy consumption as a factor of time only. However, the total energy consumption in this thesis is calculated in a different way in section 5.3 with details.

2.3. ONE BEAM DEVICE STRUCTURE

Figure 2.8. The first tunable harvester prototypes

Initially, one beam device structure is composed of a small PiezoWave® motor and a piezo coupled generating beam, see Figure 2.8. PiezoWave® motor is neat enough to place on the beam, and virtually consumes no space. It is also effectively tunes adjust the resonance frequency of the beam. The actuator shaft does not have significant mass. A movable tip mass is additionally placed right on the motor shaft for the first design.
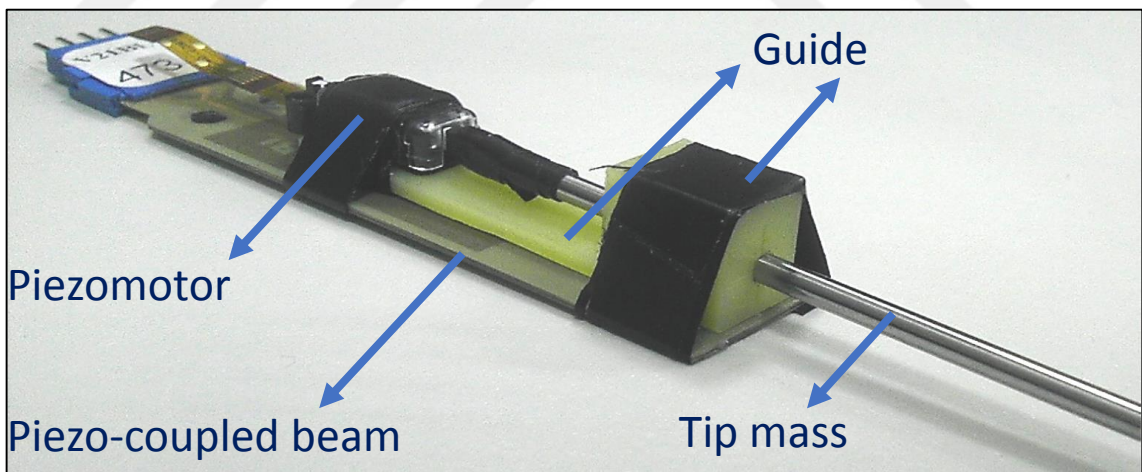
Figure 2.9. The second tunable harvester prototypes

A small Kestamid structure is built on the beam to allow for additional mass with constructions in order to eliminate transferring bending moment to the motor shaft for the second generation design, Figure 2.9.

2.4.   FINAL DEVICE STRUCTURE

The proposed VEH is shown schematically in Figure 2.10. Two off-the-shelf piezo-coupled cantilever beams [21] are used. A linear actuator is fixed to the one of the beams (called as tunable beam) and as for the tip mass, a nail is connected to the shaft of the actuator. The second beam, which is identical to the tunable beam, is employed instead of a commercial accelerometer. It has a fixed natural frequency, therefore it is referred as fixed beam.
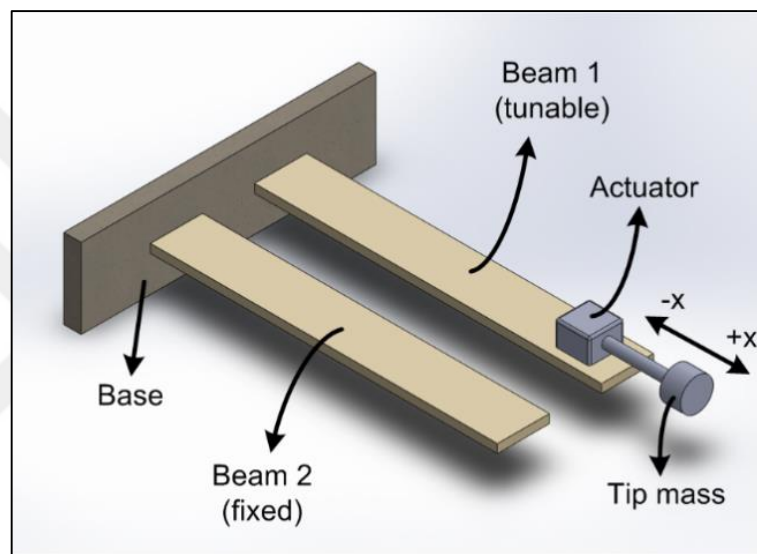
Figure 2.10. Schematic of the proposed VEH

Figure 2.11 shows a photograph of the assembled VEH. The two end positions of the tip mass are named as open and close. The close position refers to the home position of the piezomotor, where the tip mass is at the nearest position to the actuator. In this case, the natural frequency of the beam is at the highest value. On the contrary, the open position is the position in which the tip mass is at the farthest position from the actuator, and the natural frequency is at its lowest value. The outputs of both beams are connected to a low-power microcontroller unit (MCU), TI MSP 430 [23]. The MCU controls the piezomotor according to a tuning algorithm, described in the next section.
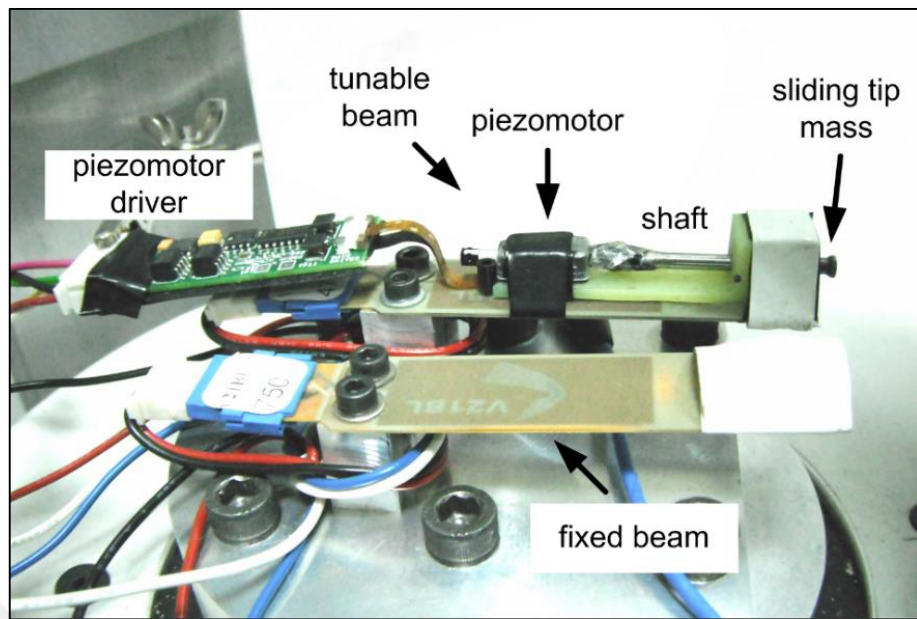
Figure 2.11. Photograph of the built device

3. TUNING ALGORITHM

The initial tuning algorithm was utilizing a blind-search based frequency tuning. The algorithm had been implemented earlier [24], and the details of the algorithm is given at the appendix. As a result of unnecessary movements involved in the method of blind-search of operation, this method is consumes additional actuation power, the method is not preferred. The preferred tuning algorithm is a phase-difference based tuning algorithm.

The aim of the tuning algorithm is to determine the moving direction of the tip mass to reach resonance. In order to determine the direction, the natural frequency of the tunable beam and the ambient vibration frequency have to be known. Calculation of the tunable beam natural frequency during operation requires the knowledge of the tip mass location relative to the actuator. However, initial experiments with the piezomotor showed that when the motor is operated in an oscillating ambient, the exact tip mass displacement in response to a known electrical pulse varies and cannot be determined, due to the varying frictional forces between the motor base and the shaft. Therefore, natural frequency of the tunable beam is treated as an unknown variable.

3.1. THE THEORY OF PHASE-DIFFERENCE BASED TUNING ALGORITHM
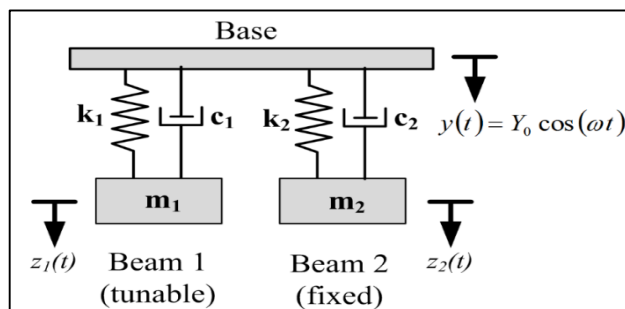
Figure 3.1. Mechanical lumped model of the VEH

A phase-difference based tuning algorithm is implemented by using the second piezoelectric beam as an accelerometer. Unlike an accelerometer, the second beam will harvest energy instead of consuming energy. Therefore, using a second beam instead of a commercial

accelerometer is advantageous in terms of energy efficiency. The proposed algorithm measures the voltage data of two beams simultaneously during operation to perform tip mass adjustment. In Figure 1.3, a mechanical lumped model of the proposed VEH is shown. The beams are represented as sprung masses, where the beam stiffnesses are represented as spring constants k_1 and k_2, and all sources of damping are represented as c_1 and c_2. Both beams are connected to the same base, which is oscillating with a single frequency ω. The tip displacement of each beam relative to the base are expressed as

$$z_i(t) = Z_i \cos(\omega t - \theta_i) \tag{3.1}$$

where

$$\theta_i = \tan^{-1}\left(\frac{2\xi_i \omega \omega_{ni}}{\omega_{ni}^2 - \omega^2}\right) \tag{3.2}$$

$$\xi_i = c_i / 2\sqrt{m_i k_i} \tag{3.3}$$

$$\omega_{ni} = \sqrt{k_i / m_i} \tag{3.4}$$

for $i = 1, 2$.

The voltage of each beam is proportional to its tip-to-base displacement $z_i(t)$. Therefore, by using the zero-crossing timestamps of both beam voltages, the external frequency ω and the phase-difference can be determined. The phase difference is given as

$$\Delta\theta = \theta_1 - \theta_2 \tag{3.5}$$

In this model, the unknown is ω_{n1}, the natural frequency of the tunable beam. Using (2)-(5), ω_{n1} can be found as

$$\omega_{n1} = \omega\left(\frac{\xi_1}{Q} + \sqrt{\frac{\xi_1^2}{Q^2} + 1}\right) \tag{3.6}$$

where

$$Q = \frac{\tan\theta_2 + \tan\Delta\theta}{1 - \tan\theta_2 \tan\Delta\theta} \tag{3.7}$$

3.2. NUMERICAL SOLUTION OF PHASE-DIFFERENCE BASED TUNING ALGORITHM

The proposed tuning algorithm requires ω and $\Delta\theta$ to be known at the time tuning algorithm is going to proceed. In this scope, these two variables forms a plane. There corresponds the third variable, which is ω_{n1}, on $(\omega, \Delta\theta)$-plane except Q is zero, see Figure 3.2. The numerical solution of the surface is narrowed to fit the working range of the VEH. The unknown natural frequency of the tunable beam forms the vertical axis as a 3-dimention surface where this variable is calculated according to **equation 6** in the previous section. The parameters ω_{n2}, ξ_1 and ξ_2 can be found experimentally using frequency sweep details are in the experimental results section in the **section 5**.
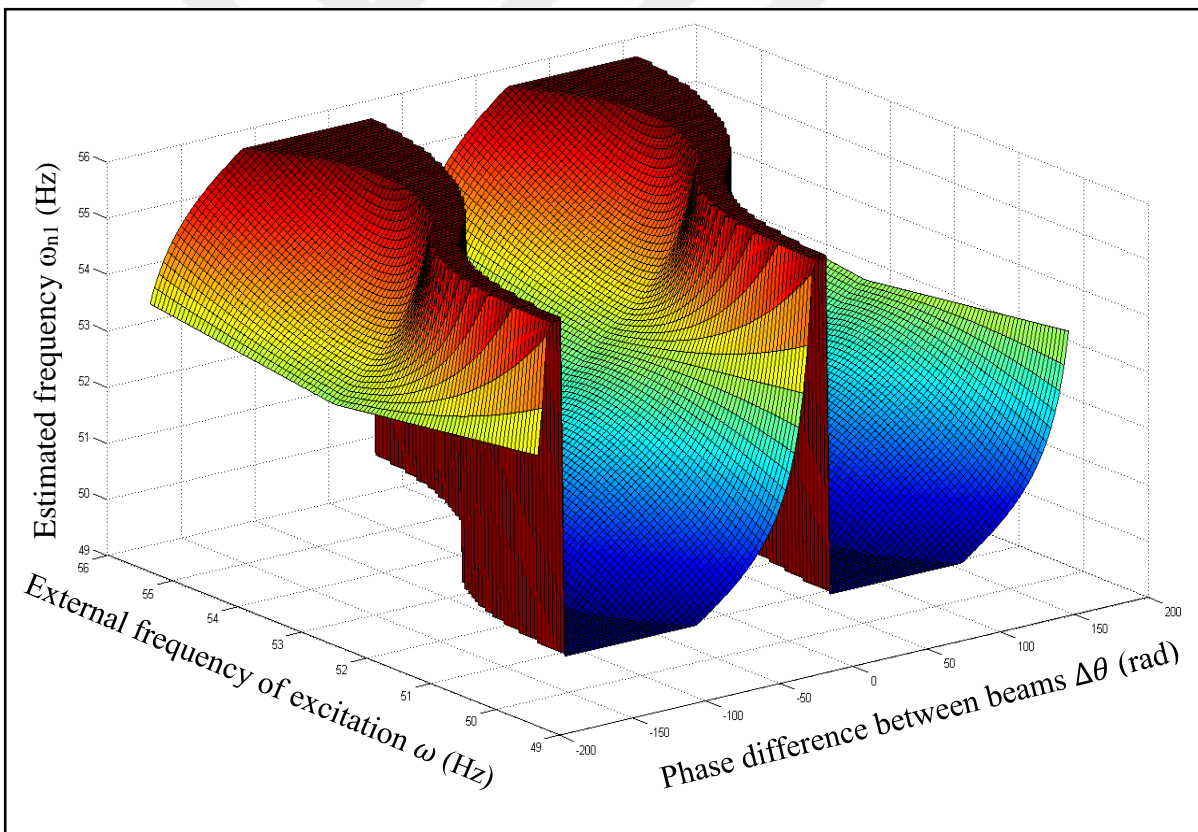
Figure 3.2. 3D control surface on the 2d plane

In the consideration tuning the natural frequency of the adjustable beam, the actuation direction has considered as the most important part. The tuning operation is based on the

sign of $\omega - \omega_{n1}$, as long as the damping ratio is low enough. Since resonance frequency of the tunable beam can be assumed to be same as the natural frequency so that the direction of tip mass motion that will move the tunable beam towards resonance can be determined. A positive $\omega - \omega_{n1}$ means ω_{n1} has to be increased by moving the tip mass towards the beam base, i.e. –x direction (refer to Figure 2.10 for directions). Likewise, negative $\omega - \omega_{n1}$, results in +x direction movement of the tip mass, see Figure 3.3 and 3.4.

Furthermore a threshold value can be set to eliminate unnecessary movements as such $\omega - \omega_{n1}$ is less than the threshold, the system is assumed to be close to resonance and the tip mass is not moved. The result can also be expressed as shading the plane with two colors for each directions similar to a map where **the red regions** on the surface indicates $\omega - \omega_{n1}$ is larger than zero and **the blue regions** indicates $\omega - \omega_{n1}$ is lower than the zero and name the surface as control surface in Figure 3.5.
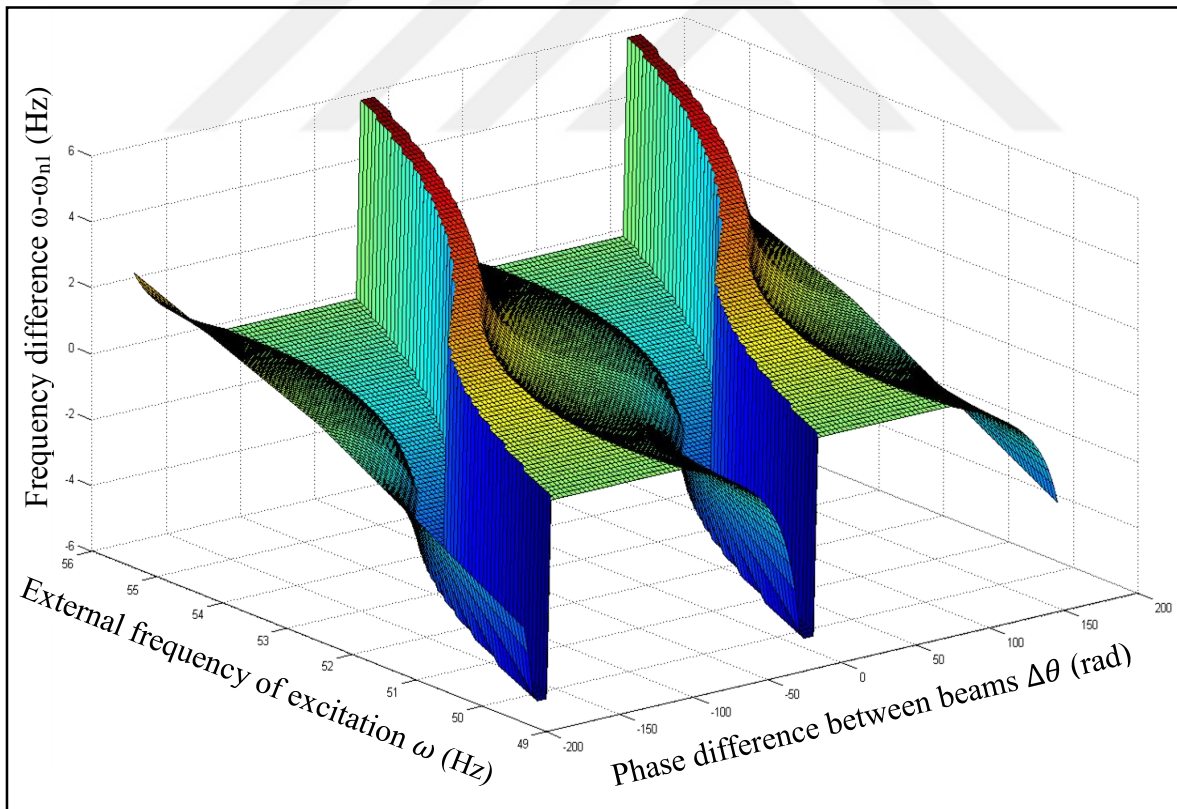
Figure 3.3. 3D view of the frequency difference (ω-ω_{n1}) on frequency-phase plane
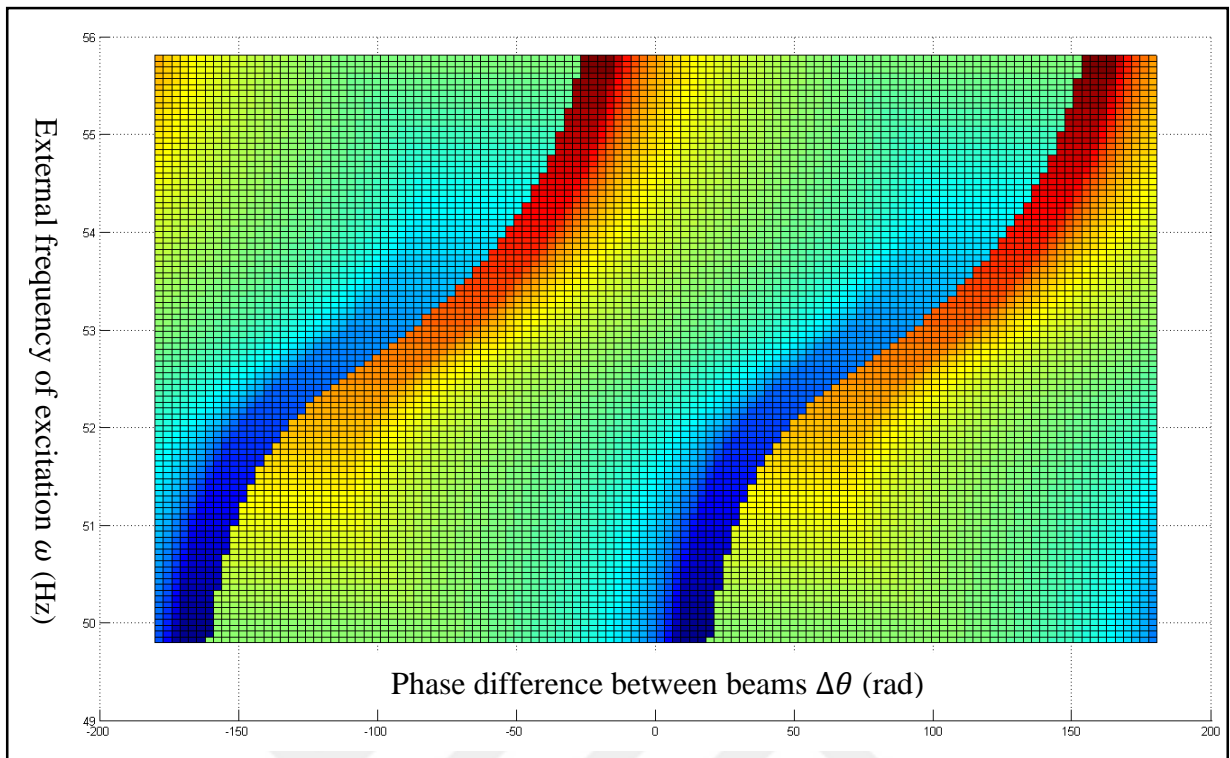
Figure 3.4. 2D view of the frequency difference (ω-ωn1) on frequency-phase plane
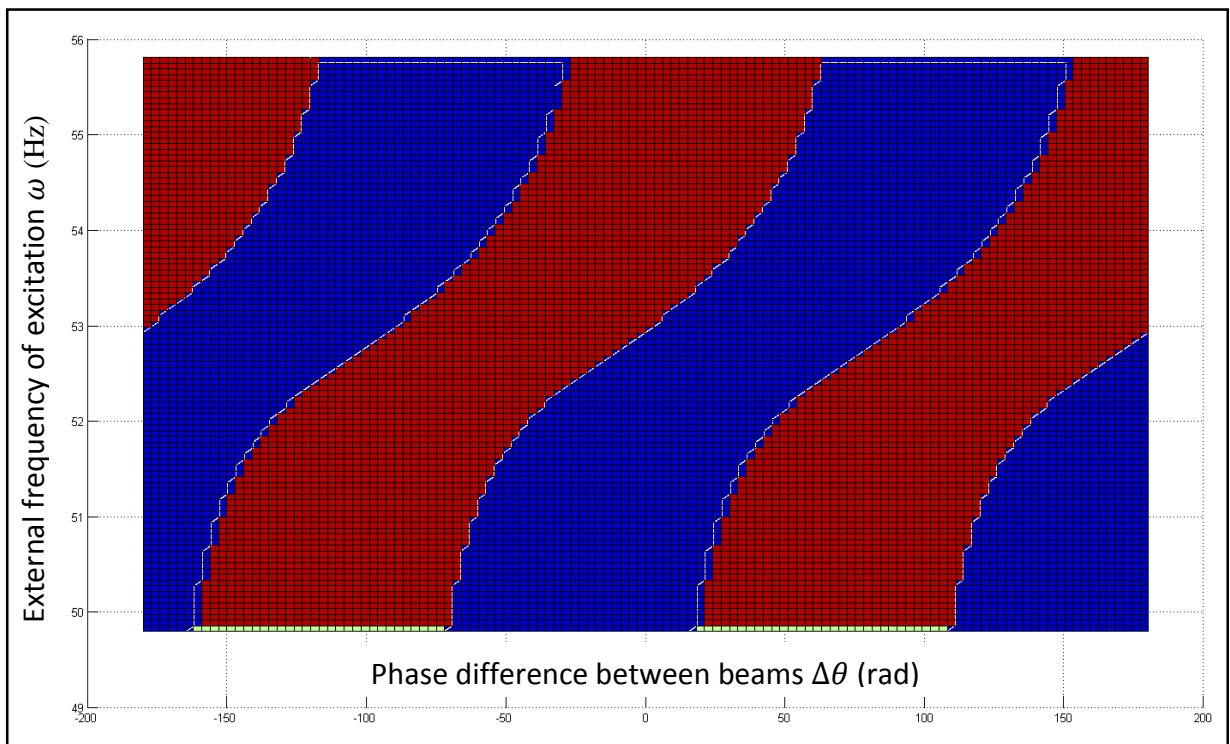
Figure 3.5. The control surface

3.3.   SENSITIVITY ANALYSIS

The shape of the control surface directly depends on the lumped parameters where any change in that parameters effects the tuning operations for the proposed tuning method shown in previous section. The MATLAB environment is used to analyze these changes numerically. The decision of the motor direction is represented as the sign of the solution on each points of the frequency-phase plane, and the simulation constants are alternated by the same amount at a time so that the alternation of the control surface can be investigated. The induced error by the alternation due to the change in the corresponding lumped parameter corresponds the dark marked points where the solution with the unchanged parameters differs from the alternated solutions by an amount of %1.
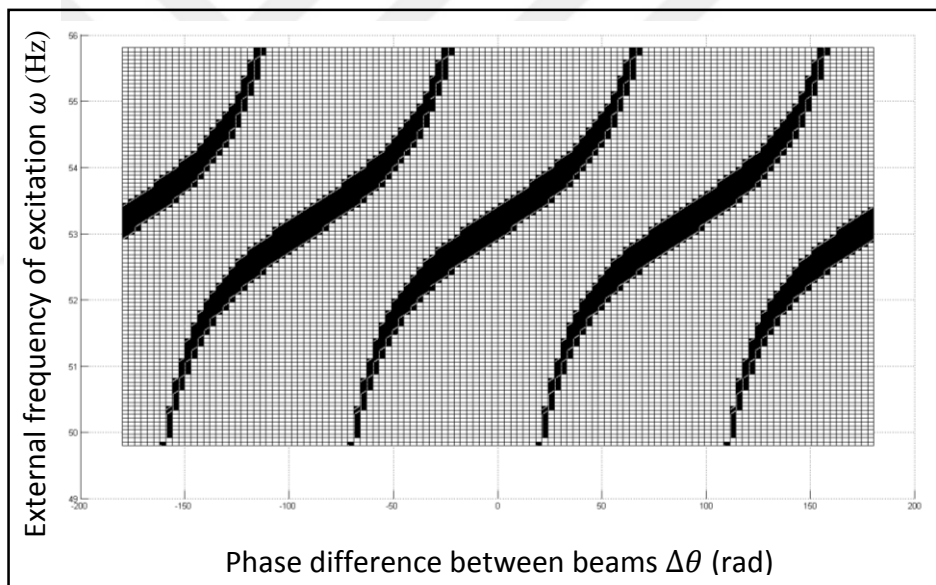
Figure 3.6. Increase in ω_{n2} (fixed beam) by %1

On the first graph, see Figure 3.6, there is %13 error for ω_{n2} which is the natural frequency of the fixed beam and the same amount of change in ξ_2 resulted by amount of less than %1 on Figure 3.7 for the control surface sensitivity. The change of ξ_1, which is the damping ratio of the adjustable beam, gives no dark points in the simulation results to show. Both of the range and the quantization noise impress the results but these behaviors are analogous to the MCU's controller behavior. These results indicates that the natural frequency of fixed beam ω_{n2} has to be determined precisely and the algorithm is fairly insensitive ξ_1 and ξ_2.
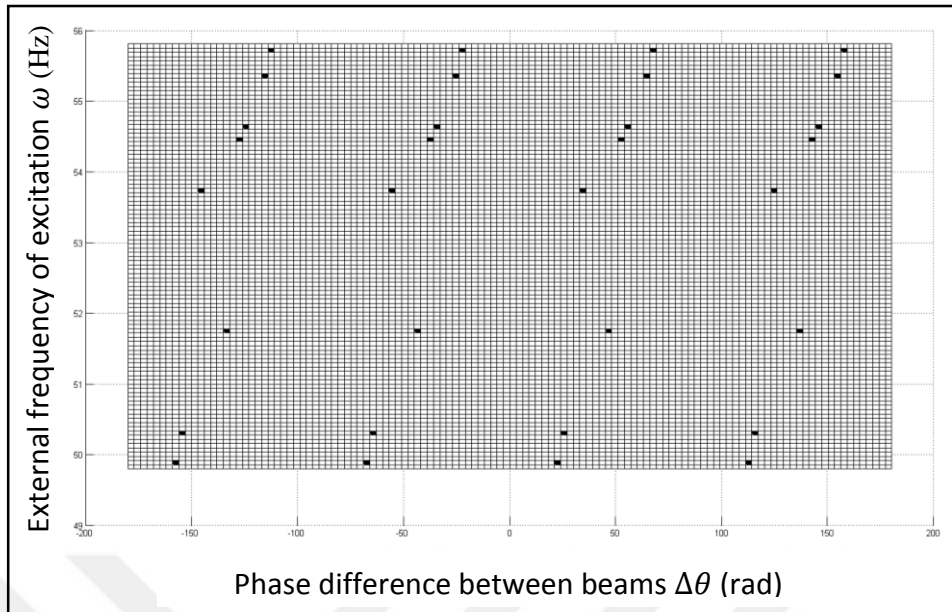
Figure 3.7. Increase in ξ_2 (fixed beam) by %1

4. CONTROLLER UNIT AND ELECTRONICS

4.1. SIMPLIFICATION OF THE PHASE-DIFFERENCE ALGORITHM

Exact implementation of the proposed tuning algorithm is bulky for MCU, and also there is no need to implement all of the control surface. The motor direction is merely required to tune the adjustable beam. Therefore, an approximate solution is proposed to implement the phase based tuning algorithm to the MCU. The solution is found by mapping the current control surface to a simplified one which uses integer values without any floating point operations. The intention is to lower the required computation time. Consequently, it gives an opportunity to lower the CPU frequency that directly gives the flexibility of lowering the supply voltage of the MCU. Therefore, it also significantly reduces the energy consumption of the VEH. As for simplification, any $(\Delta\theta, \omega)$ measurement can be converted to $(\Delta\theta', \omega)$ with the use of the formula below:

$$\Delta\theta' = c_1 \Delta\theta + \frac{c_2\omega + c_3}{\omega^2 + c_4\omega + c_5} + c_6 \qquad (4.1)$$

With the use of genetic algorithm, the coefficients of the equation 8 (c_1 to c_6) are determined so that each region on the virtual control surface can be expressed as rectangles and also every distance between any regional margins can be exactly 2^{12} bits (4096 in integer). The most notable thing is the 13th bit since it gives the sign of $\omega - \omega_{n1}$ which is the motor tune direction. The simplified version of the algorithm practically predicts the direction to tune the VEH in the same way that analytical solution does; it takes $\Delta\theta$ and ω and gives the required motor direction to tune the beam.
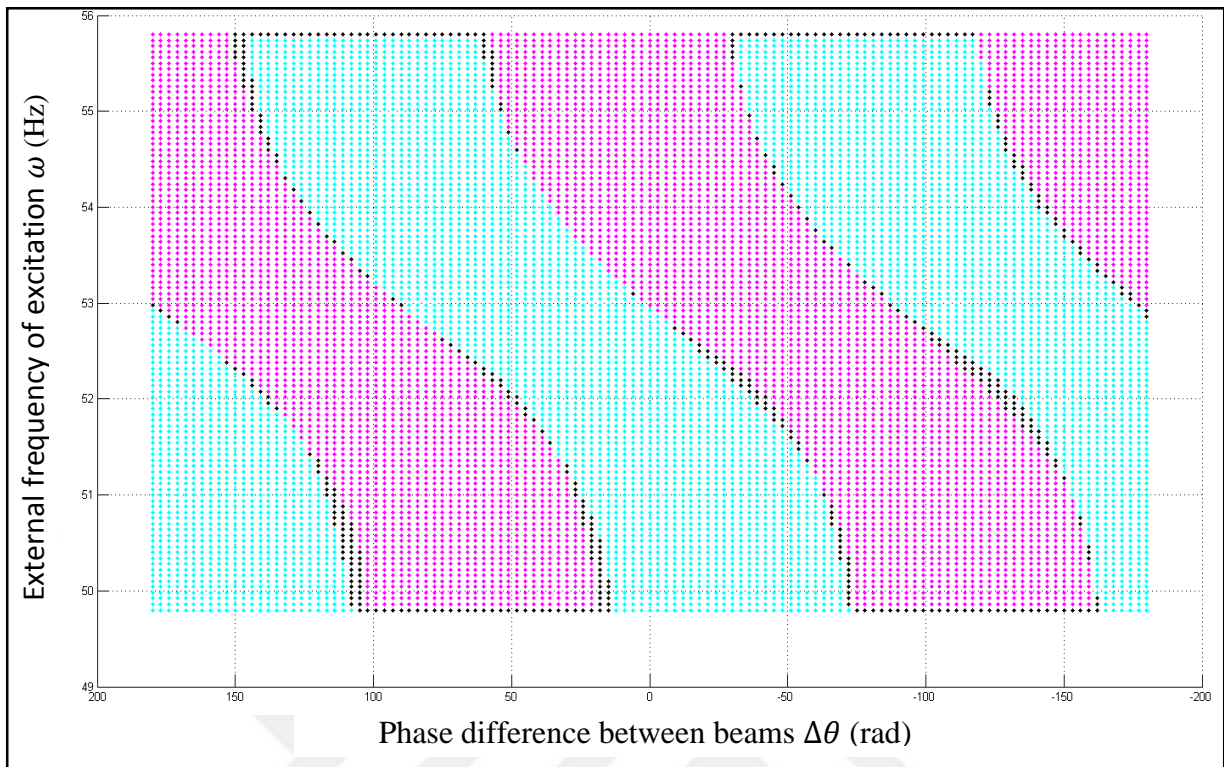
Figure 4.1. Error introduced by using simplified tuning algorithm

Due to the repetitive behaviors of the control surface, the first 13 bit from the right hand side has significance where 13th is used to determine motor direction. The proposed formula has also the ability to compensate the MCU's unit conversion. The opportunity of not using additional unit conversions operations is further decreases the number of calculations. Figure 4.1 shows the validity of the conversion method at which the marked points with black indicate the error when the solution of the analytic expression and the simplified tuning algorithm is not matched, see Figure 4.2. The amount of the error promotes the movement threshold where motor should not move accordingly.
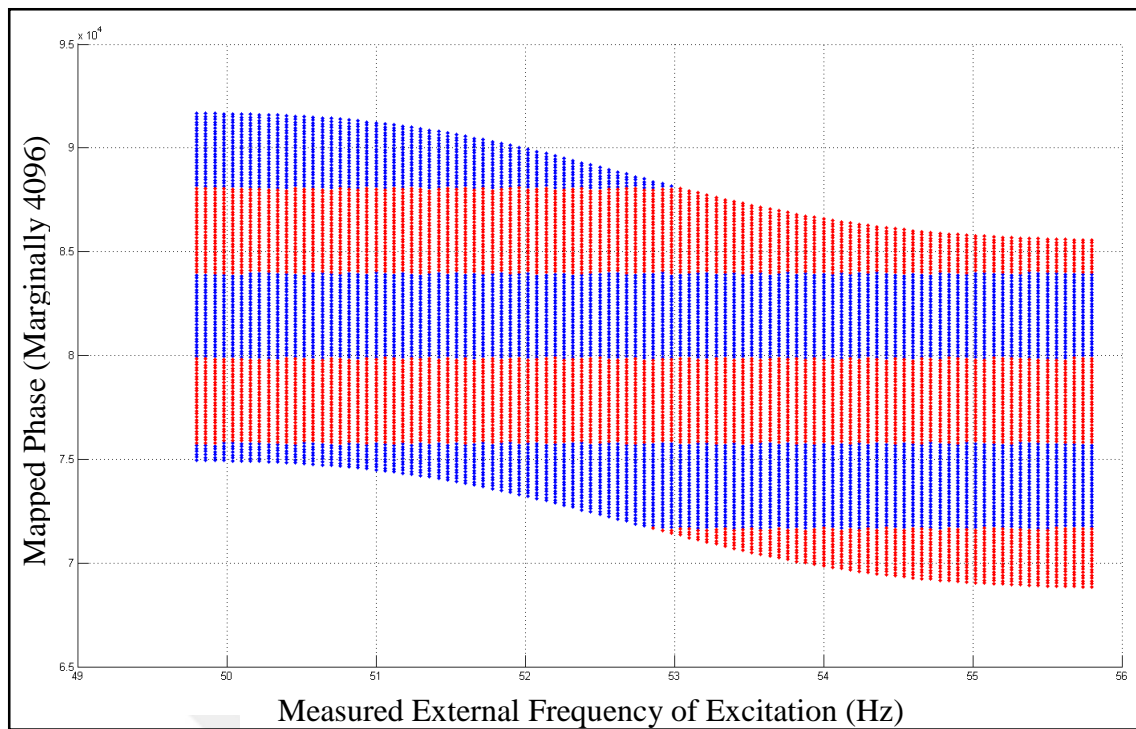
Figure 4.2. The fully mapped tuning algorithm

4.2. CONTROLLER UNIT IMPLEMENTATION OF THE ALGORITHM

The algorithm implementation is depicted as a flowchart in Figure 4.3. An ultra-low-power MSP 430 series MCU is used [23]. During operation, the MCU is mostly in a power-saving sleep state, in which the CPU and most of other modules are off. The watchdog module of the MCU periodically waits for a predefined time interval, called the deep sleep period, and then sends a wake up interrupt to the CPU. When the CPU is awaked, phase measurement is performed ensuring that there is enough energy with the help of P_{good} signal from one of the voltage converts which will be explained in harvester electronics section.
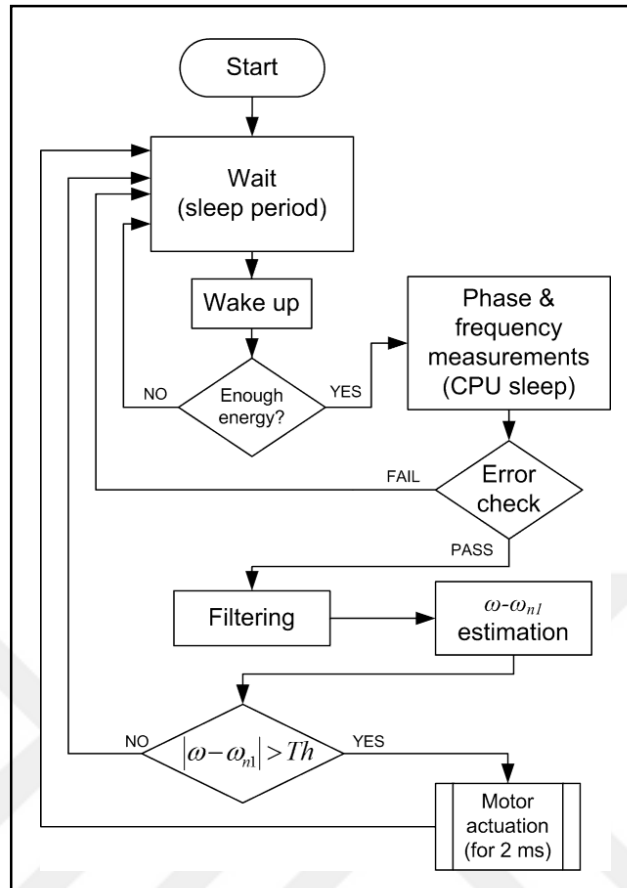
Figure 4.3. Algorithm flowchart

4.2.1. PHASE MEASUREMENT IMPLEMENTATION

The phase measurement step mostly consists of waiting for a level-crossing event from the comparator module and storing the timestamp of the corresponding event step. The comparator module compares the beam output voltage with a small reference voltage and changes sign when one voltage exceeds the other. With this method, phase difference $\Delta\theta$ and frequency ω can be calculated. The timer and the comparator modules of the MCU are on, whereas the CPU, the major energy consuming module, is mostly off during this step. Therefore the overall energy consumption of the MCU is very low during phase measurement.
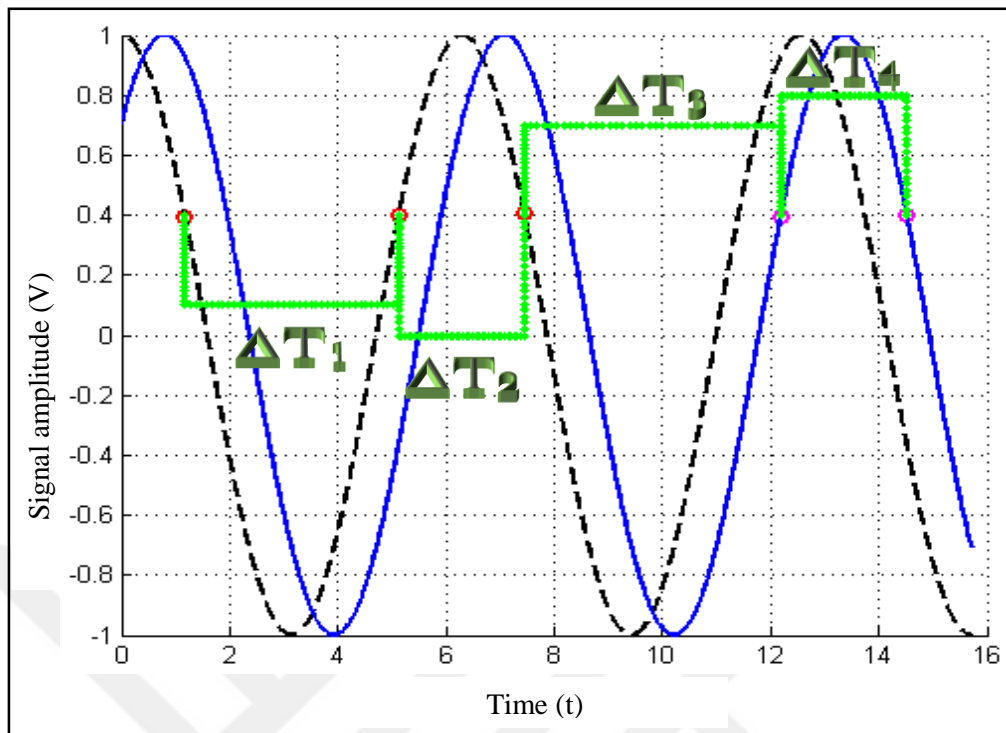
Figure 4.4. Phase reading and time stamps

The phase and frequency estimation is based on recording of 5 time stamp where the potential difference between corresponding terminals crosses a certain value, see Figure 4.4. Only one comparator is used to produce an interrupt to enable the CPU and the CPU records the corresponding time stamp. Every time stamp links a channel and an edge direction given in Table 4.1. The phase reading starts with a down edged interrupt on the first channel. The following timestamps are stored by a state machine retaining a timeout value. Moreover, any time stamp, which are out of bounds, produce instability flag. Therefore the difference between subsequent time stamps are calculated and compared with similar ones.

Table 4.1 Time stamp condition

Timestamp	Condition
T1	Channel A down edge
T2	Channel A up edge
T3	Channel A down edge
T4	Channel B up edge
T5	Channel B down edge

If any of the stability flag are not falsely marked, the average value of the each signal couple is used to calculate frequency, signal_1 and signal_2, is respectively written in 3xn measurement matrix where "n" is the size of the filter taken as ten. The frequency information is kept as the summation of the first and the second time differences which is the period in MCU's tick unit as the resultant settings of the timer and the oscillator modules, likewise the positive phase ratio in integer is estimated via the formula below:

$$D_1 = \Delta T_1 + \frac{\Delta T_2}{2} \tag{4.2}$$

$$D_2 = \Delta T_3 + \frac{\Delta T_4}{2} \tag{4.3}$$

$$\Delta\theta = D_2 - D_1 \tag{4.4}$$

4.2.2. FILTERING AND DIRECTION ESTIMATION

After sufficient amount of phase and frequency measurements are obtained, an error check is performed by calculating the variance of the measurement array. If the variance is below a threshold value, the measurement is considered as correct. This variance is then used to reduce noise by eliminating outliers at the filtering step in this section.

It is observed that the phase estimation has large jumps. Before MCU implementation of the filter for each time stamp of the measurement matrix, the filter is first tested on only the phase readings directly estimated by the MCU. Therefore the vector that contains recorded measurements are filtered by the formula below:

Simple average;
$$\mu = \frac{1}{n}\sum_{i=1}^{n}(v_i) \tag{4.5}$$

Error squares;
$$E_i = (v_i - \mu)^2 \tag{4.6}$$

Half square error;
$$\alpha = \epsilon + \frac{1}{2*n}\sum_{i=1}^{n}(E_i) \tag{4.7}$$

Elimination of outliers;

$$\beta_i = logical(E_i < \alpha) \tag{4.8}$$

Partial sum of outlier free data;

$$p = \frac{1}{[\sum_{i=1}^{n}(\beta_i)]} \sum_{i=1}^{n}(\beta_i * v_i) \tag{4.9}$$

Where v_i is a row of the measurement matrix, p is the corresponding value and ϵ is an upper bound on the relative error due to rounding in floating point arithmetic, taken as 1 in this case. Therefore p is calculated upon the given input vector v_i.
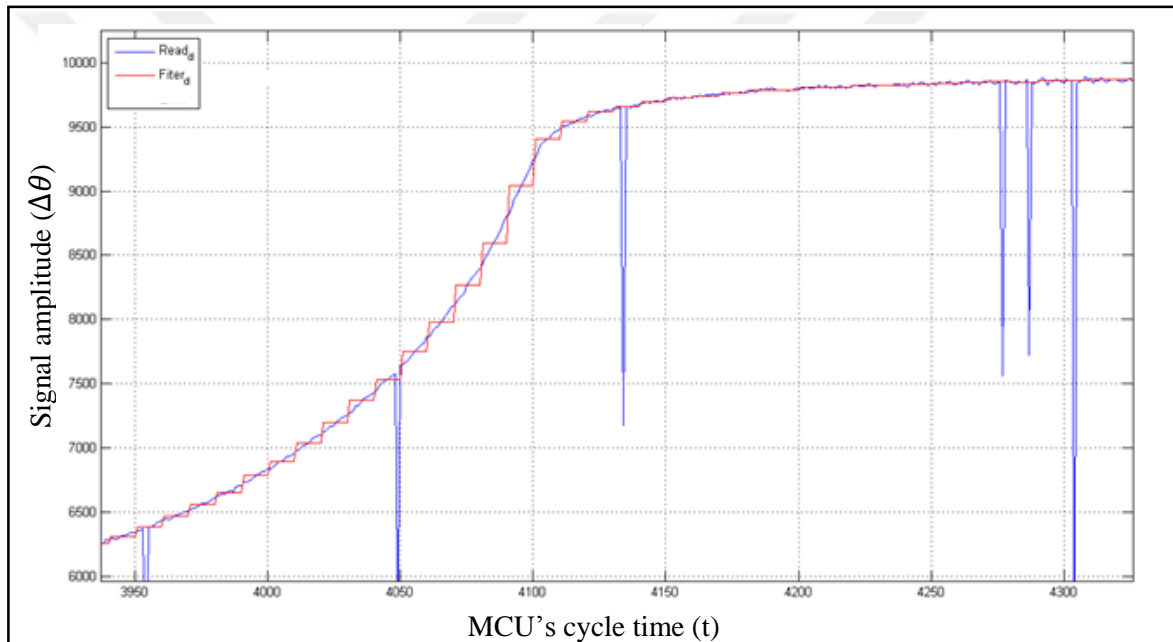
Figure 4.5. Raw and filtered phase data

After the robust outlier elimination on the data by the filter is demonstrated via the same algorithm running on MATLAB. On the phase reading see Figure 4.5, the source of the noise was investigated. When a sharp noise happens on the non-filtered data points, the memory of the MCU was checked for error. Paper and salt noise was found on the measurement matrix of the MCU's memory. Since the proposed tuning algorithm is sensitive to the frequency and phase measurements, proposed outlier reduction filter is applied to each of the three rows of the measurement matrix on the MCU before evaluating phase difference rather than the phase estimations. The impulsive kind of noises were no longer observed during debug sessions on the MCU's phase measurements.

4.2.3. PIEZOWAVE® ACTUATION

After filtering, the difference between the external frequency and the tunable beam natural frequency $\omega - \omega_{n1}$ is calculated with the help of simplified version of equation (6). The sign of this difference determines the direction of the tip mass motion according and the simplified version of the algorithm is implemented to the VEH. If the absolute value of the difference is above a threshold value, the piezomotor is actuated for a fixed duration of 2 ms. Otherwise, no action is taken and the system again gets into sleep state until the next interrupt by the watchdog module.
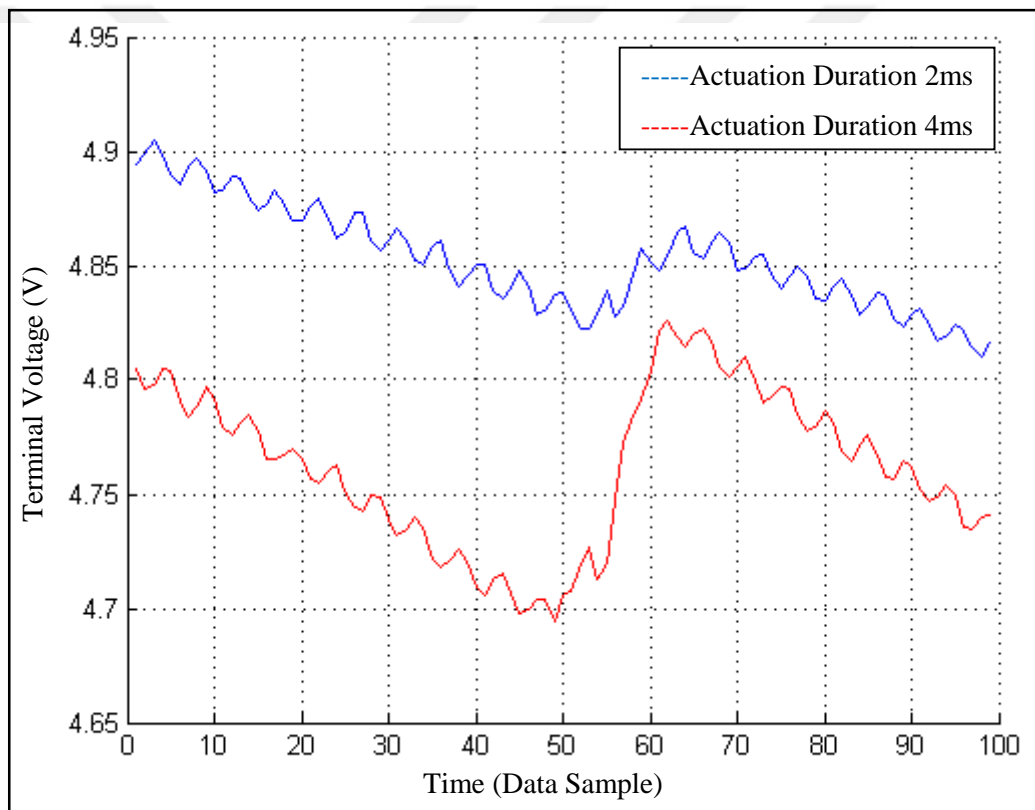
Figure 4.6. Effect of Step duration

The controller of the PiezoWave® motor also includes a micro controller. The supply voltage of the motor controlled board is controlled on demand for the elimination of the unnecessary power consumption. When motor actuation is required, the motor controller switched on for a certain amount of time. This controls the duration of the motor movement and the travel distance of the tip mass accordingly. Analysis of the duration of one actuation

duration becomes chaotic due to the fact that the distance of the tip mass traveled is very inconsistent due to varying frictions. The main reason of this varying friction is the vibration of the whole structure. Initial experimentations showed that two millisecond of actuation is an adequate stepping duration since under one millisecond of actuation might causes the tip mass not to move whereas more than 4 milliseconds of actuation time lowers the tune accuracy. In Figure 4.6, the effects of 2 and 4 milliseconds of actuation duration on a sweeping excitation are compared where the size of voltage jump indicates similar shifts in the resonance frequencies of the beams.

4.3.   HARVESTER ELECTRONICS

The electronics of the harvester is shown in Figure 4.7. The harvested energy has to supply the MCU and the piezomotor driver when necessary. For converting the unconditioned voltage from the beams to DC voltage, LTC 3588 AC/DC converters are employed [25]. LTC 3588 has four available output voltage selections (1.8, 2.5, 3.3 and 3.6 volts). The piezomotor driver requires at least 3.2 V supply, whereas the MCU voltage supply can be between 1.8 V and 3.6 V [23]. The current implementation of the algorithm runs the CPU at 8 MHz which requires at least 2.2 V supply to the MCU. Instead of both feeding the piezomotor driver and MCU with the same DC voltage supply, it is decided to supply 2.5 V to the MCU, to decrease its energy consumption. Therefore, two LTC 3588 chips with separately set output voltages are placed. The LTC 3588 chip named LTC 3588–A supplies the piezomotor driver whereas LTC 3588-B supplies the MCU. Each LTC 3588 chip has its on-chip rectifier; therefore no separate rectification circuitry is built. In addition to the LTC 3588 connection, each beam has a connection to the microcontroller for phase and frequency measurements required for the tuning algorithm.

A 440 µF storage capacitor is connected to the ends of the LTC 3588 rectifiers. In addition, smaller capacitors are connected prior to the MCU and the piezomotor driver, respectively, for the purpose of smoothing their input voltages. The piezomotor driver is powered when the MCU decides to move the tip mass, with the help of a switch transistor. There is a voltage drop of 0.4 V across the switch transistor, so the output voltage of LTC 3588–A is set to 3.6 V. This way, 3.2 V supply to the piezomotor driver is ensured. The MCU performs the

energy level check by reading the PGOOD pin on the LTC3588-A. The PGOOD gives logic high if the output voltage of LTC 3588-A is above ~3.4 V [25]. The MCU has also a direct connection to the piezomotor driver to send the tip mass movement direction. There are also several electrical measurement probes to monitor the capacitor voltages during experimental study, in which the internal resistances of these measurement probes use the harvested energy as well. The external load is connected to the storage capacitor.
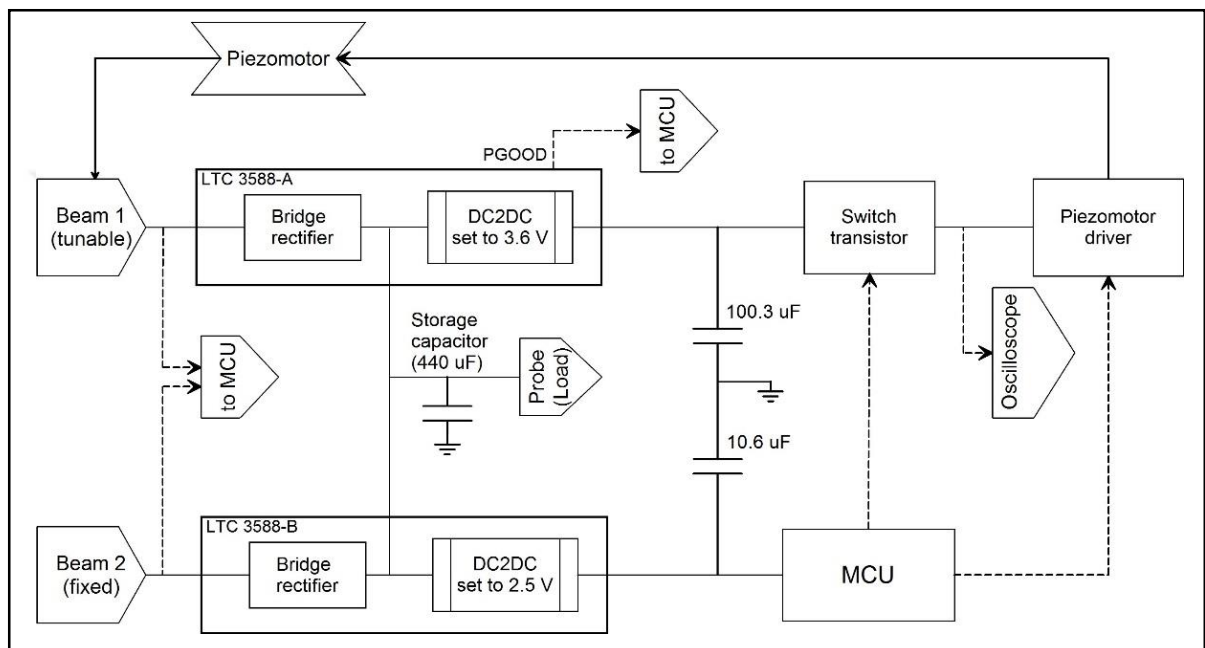

Figure 4.7. Power harvesting electronics. Signals are shown with dashed lines

5. EXPERIMENTAL RESULTS AND DISCUSSION

5.1. INITIAL CHARACTERIZATION

The initial characterization involves determination of the lumped model parameters (ω_{n2}, ξ_1 and ξ_2) and the limits of the tunable beam natural frequency (ω_{n1}). The output of the tunable beam is connected to a 22 kΩ load resistance, and the RMS voltage across the resistance is recorded during frequency sweep, realized by a permanent magnet shaker. The experiment is performed at four tip mass (nail) positions: closed, mid-closed, mid-open, open. The nail tip to cantilever base distance is shortest at the closed position (61 mm), longest at the open position (69 mm), and has intermediate values at the other two positions (~64 mm at mid-closed and ~66 mm at mid-open).

The frequency responses at these four positions, together with the frequency response of the fixed beam are shown in Figure 5.1. The fixed beam natural frequency is calibrated so that its natural frequency is within the tunability range of the tunable beam (~53 Hz). The frequency sweep directions are shown with arrows. As seen from Figure 5.1, the tunable beam exhibits a significant hysteresis, whereas the fixed beam exhibits a fairly linear behavior. In addition, the response shapes of the two beams are different. The tunable beam response is fairly steep below resonance, compared to a more flat response of the fixed beam. The response shape and hysteresis of the tunable beam are signs of its inherent nonlinearities, which is due to the added piezomotor and the tip mass.

The tuning algorithm described in section 3.1 requires both beams to be treated as linear spring-mass-damper systems. The nonlinear behavior of the tunable beam causes difficulties in calculating its damping ratio. Fortunately, the algorithm estimates the piezomotor direction by using the phase angle between the beams and the phase angle is fairly insensitive to the tunable beam damping ratio. Therefore, we do not expect the nonlinearity of the tunable beam response to result in mistuning.
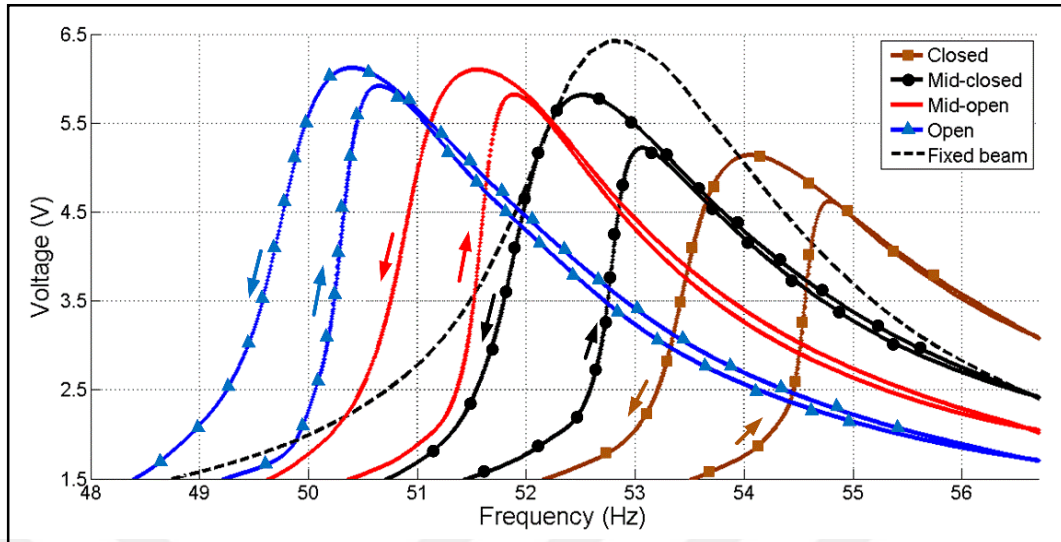
Figure 5.1. Frequency response of the fixed beam and the tunable beam
at various tip mass positions. The fixed beam response is given
as a single curve due to its negligible hysteresis

5.2. TUNING PERFORMANCE

Once the lumped model parameters are obtained with the experiment described in the previous section, we use them as input parameters of the tuning algorithm implemented on the MCU. The tuning algorithm is then tested via a frequency sweep test. The power budget is not considered in this experiment, therefore the harvester is connected to an external power supply and the tunable beam is connected to a 22 kΩ load resistance. The sleep period of the MCU is set to 4 seconds. In other words, the algorithm calculates $\omega - \omega_{n1}$ value, and if this value is above the threshold, the tip mass is moved accordingly based on the sign of $\omega - \omega_{n1}$ at every 4 seconds. The piezomotor actuation duration is kept fixed as 2 ms. The MCU measurements are monitored via a computer interface. Simultaneously, a separate DAQ system records the voltages of both beams at 10 kHz sampling rate. The waveforms and the phases of the two channels are also investigated with an oscilloscope and compared with the MCU measurements.

Figure 5.2. The frequency response with and without tuning. The sweep rate is 1.03 Hz/min. The sleep period for the self-adaptive response is 4 seconds

In Figure 5.2, the frequency response of the tunable beam is plotted while the tuning algorithm is running. For comparison, the response of the same beam at mid-open position, without running the algorithm, is given as well. The shaker frequen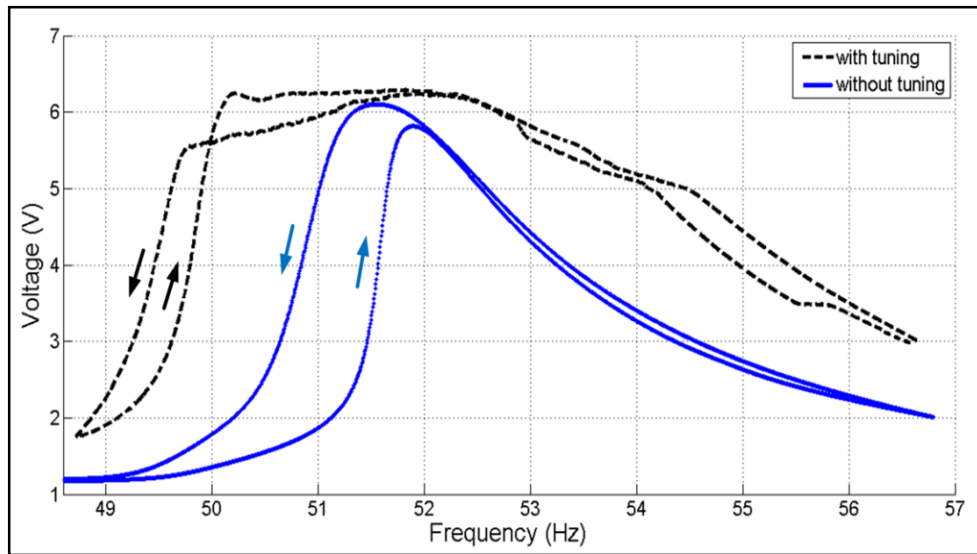cy is swept between 48.6 Hz and 56.6 Hz, at a sweep rate of 1.03 Hz/min. As seen, the algorithm is able to tune the tip mass position successfully with low hysteresis. The non-adaptive response exhibits a steep resonance curve with significant hysteresis. On the other hand, the self-adaptive response exhibits a plateau between 50-54 Hz.

The bandwidth is calculated by taking the average responses to positive and negative sweep and then by applying the half-power bandwidth method to the averaged response. The half-power bandwidth of the self-adaptive response is calculated to be 5.13 Hz, which is 3.13 Hz higher than the bandwidth of the non-adaptive response. The fractional bandwidth, which is defined as the bandwidth over center frequency, is found to be ~10% for the self-adaptive case and ~4% for the non-adaptive case. The comparison can also be done between a slightly wider analytically best tune, see Figure 5.3. The result are visually similar but the improvement in bandwidth is directly limited by the 8 mm piezomotor motion range, constrained by the manufacturer. A piezomotor with a longer motion range can lead to better improvement in bandwidth with the same tuning algorithm.
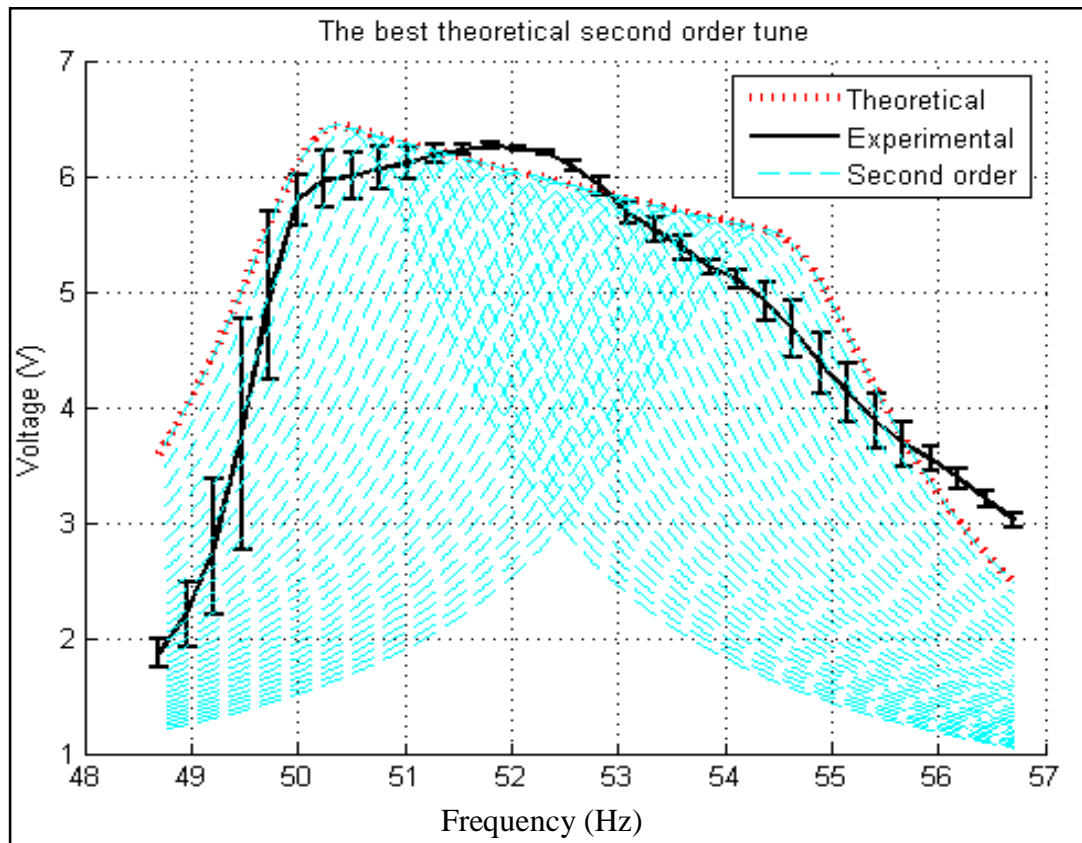
Figure 5.3. Analytical solution of the best tune with the fractional bandwidth of 6 Hz

The sweep test is repeated with different sweep rates and sleep periods, to examine the effect of the parameters in tuning performance. In Figure 5.4, the tunable beam response is plotted for sleep periods of 4 and 16 seconds, both having the same sweep rate of 1.03 Hz/min. At a sleep period of 4 s, the natural frequency of the tunable beam is tuned frequent enough, whereas at a sleep period of 16 s, the tunable beam natural frequency is too slow to be able to catch the sweep. At high sleep period, the tunable beam catches resonance at different frequencies at positive and negative sweeps. This leads to a significant hysteresis in the response. The value of peak frequencies at the positive and negative sweep are not absolute, as they depend on the beam natural frequency at the beginning of the sweep test.

Figure 5.4. The effect of MCU sleep period on tuning performance.

The sweep rate is 1.03 Hz/min

Figure 5.5. The effect of sweep rate on tuning performance.

The sleep period is 4 seconds

The effect of sweep rate on frequency response is given in Figure 5.5. This time, the sleep period is kept fixed as 4 seconds, and the experiment is performed as the sweep rate is quadrupled to 4.12 Hz/min. As seen, increasing either the sweep rate or the sleep period has a similar effect on the performance of the algorithm. When the sweep rate is high (4.12 Hz/min), the tunable beam can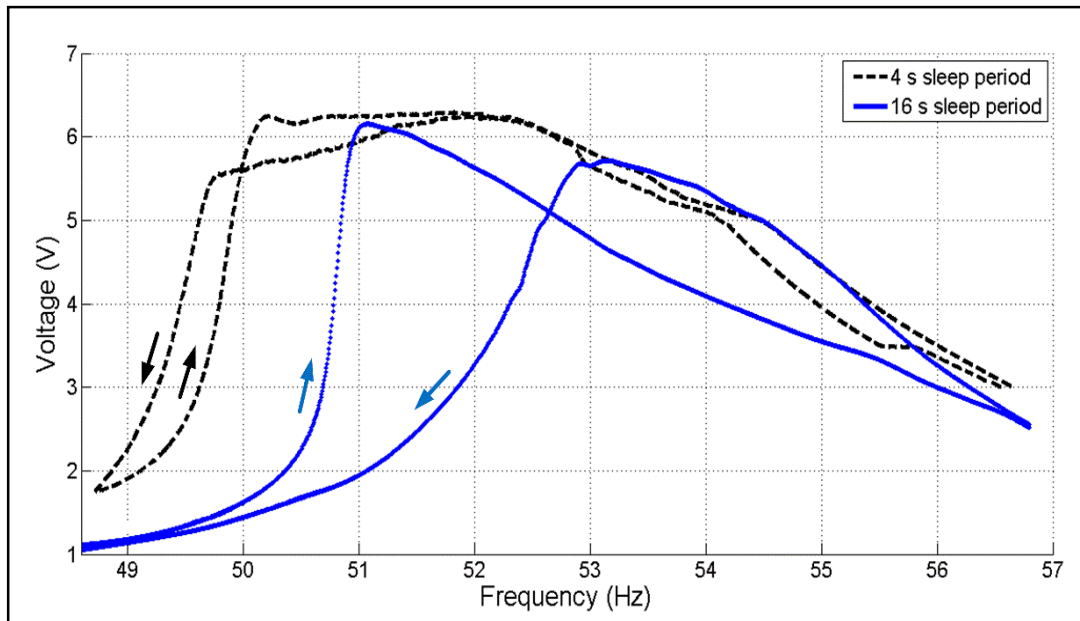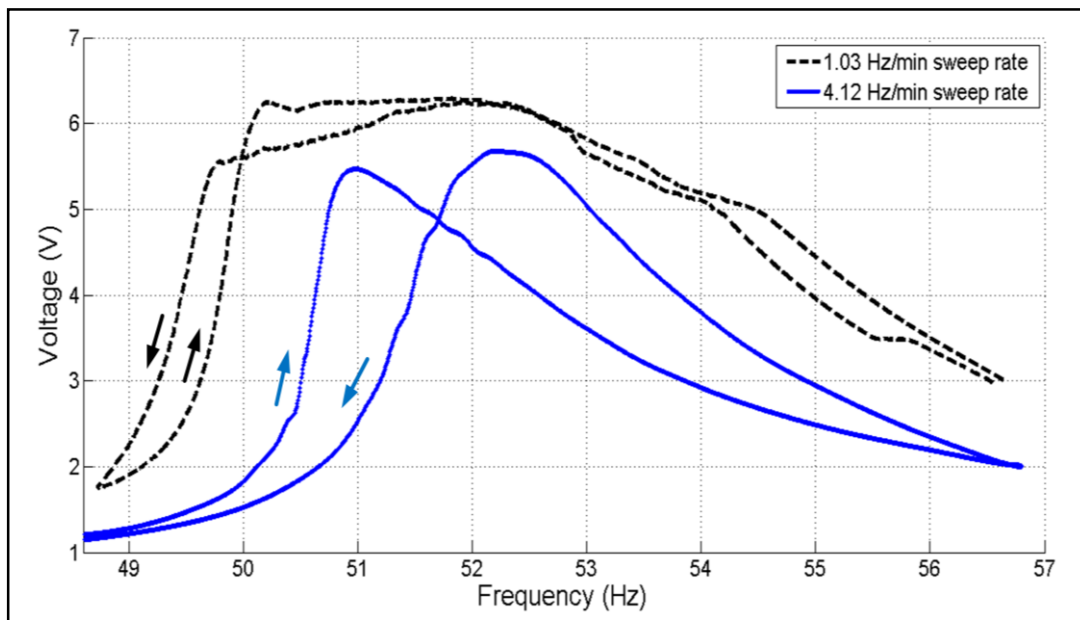not reach the frequency sweep, whereas a lower sweep rate results in successful tuning. Therefore, the performance of the algorithm is limited both by the sweep rate and the sleep period.

However, comparing Figures 5.4 and 5.5 leads to the observation that increasing the sweep rate deteriorates the tuning performance more, compared to increasing the sleep period. To explain this, it is hypothesized that at high sweep rate, the beams do not have enough time to accumulate much charge at their electrodes, resulting in poor harvesting efficiency. Finally, it should be noted that lowering the sleep period will result in increased power consumption. The power budget and self-sufficiency of the harvester is investigated in the next section.

5.3. POWER DISTRIBUTION AND SELF-SUFFICIENCY

In order to test the self-sufficiency of the harvester and to determine the average power demand of system components, the harvester is disconnected from the external power supply and connected to its electronics given in Figure 4.7. The time response of the storage capacitor voltage is recorded during a discharge and recharge experiment at resonance. During the experiment, the tuning algorithm is modified to move the tip mass once in every 4 seconds. In fact, there is no need to move the tip mass as the system is at resonance and the ambient frequency is not varying. The reason for periodically moving the tip mass is to clearly see the effect of frequent piezomotor actuation in the power budget. Therefore, it will be possible to foresee the overall power consumption if the ambient frequency was varied. The measurement circuitry of the probe used in monitoring the storage capacitor voltage is assumed to be the external load of the system, since the voltage divider of this circuitry consumes significant amount of energy. Using this probe as load has already been depicted in Figure 4.7.

Figure 5.6 shows the storage capacitor voltage level as a function of time. The experimental procedure can be explained as follows: Starting with a storage capacitor fully charged at its maximum voltage of 20.5 V, the mechanical shaker is started with 1.05 gn acceleration at a constant frequency of 53 Hz. The natural frequencies of both beams are set to 53 Hz in this case. Then the shaker is turned off, and after the storage capacitor voltage decreases to ~9 V, the shaker is turned on again with the same configuration (53 Hz, 1.05 gn). The experiment finishes after the capacitor is again totally charged by the harvester. The time when the shaker is stopped and restarted can be clearly observed from Figure 5.6. The tiny periodic pulses on the voltage plot are due to the piezomotor actuation once in every 4 seconds. As seen from Figure 5.6, once the shaker is turned off, the storage capacitor keeps supplying the MCU and the piezomotor for around 50 seconds. When the shaker is restarted, the harvester is able to fully charge the capacitor to its maximum from 9 V, again in around 44 seconds. This demonstrates the self-sufficiency of the harvester: In a vibrating ambient, the device can simultaneously charge a storage capacitor, supply power to a load and periodically actuate the piezomotor, without requiring any external energy sources.

The theoretical power consumption of the MCU can be calculated by interpolating energy curves of the active modules including CPU of the MCU via documentation. The product documents also provides general energy consumption of the MCU at different working states, such as sleep states. Combining these information with proposed tuning algorithm gives the estimated ideal MCU power consumption estimation.
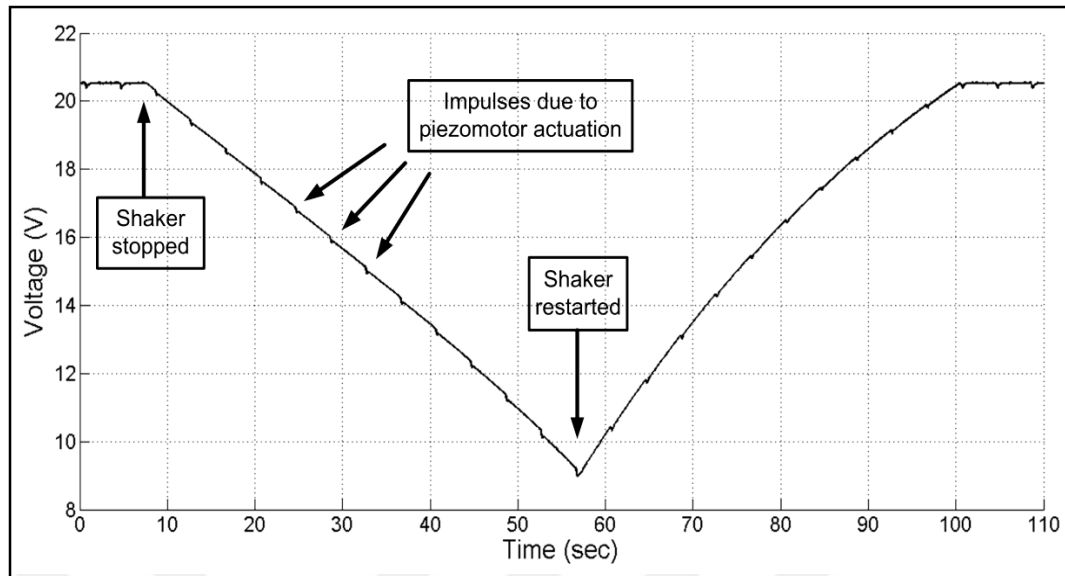
Figure 5.6. Storage capacitor voltage time response in the discharge-recharge experiment

The distribution of power consumption is given in Table 5.1. The table is constructed using the storage capacitor voltage data in Figure 5.6. From the slope of the decaying capacitor voltage after the shaker is stopped, the total power consumption of the system is calculated, as the system is not harvesting energy. On the other hand, the slope of the increasing voltage after the shaker is started gives the net power, i.e. the total harvested power minus all losses and power delivered to the load. The power consumption of the MCU is calculated using the MSP 430 data sheet [23] and the power supplied to the load is calculated using electrical circuit theory. As seen from row 2 of the table, around 3.38 mW is harvested at 53 Hz, 1.05 gn ambient vibration. The power consumption by the measurement probe, which represents power delivered to a connected load, is calculated to be 0.77 mW.

The MCU power consumption is found to be 0.57 mW, the average piezomotor actuation power demand is measured as 0.12 mW and the other losses, which includes the DC to DC converter losses and capacitor leakages, are found as 0.43 mW. The power delivered to the storage capacitor is measured as 1.49 mW. The power values given refer to the case of constant ambient frequency. If the ambient frequency is varied, the power consumption parameters are expected to be very close to the constant ambient frequency case. However, the total harvested power strongly depends on tuning performance, which in turn is related

to the sweep rate as well as the sleep period as presented in section 5.2. Therefore, it is not possible to construct a power budget table for the varying frequency case.

Table 5.1. Power distribution at 1.05 gn excitation at 53 Hz. The tunable beam is at resonance. All units are in mW

Component	Power (mW)
Total harvested Power	3.38
MCU consumption	0.57
Piezomotor consumption	0.12
Remaining electrical losses	0.43
Power supplied to extra load	0.77
Power supplied to storage capacitor	1.49

The power consumption of the piezomotor can be observed as impulsive voltage drops on the storage capacitor voltage, as observed in Figure 5.6. A closer look at these impulsive drops is provided in Figure 5.7. The energy consumption at each piezomotor actuation is found to be 0.48 mJ. This value is calculated via the expression $(1/2)C(V_1^2 - V_2^2)$, where C is the storage capacitor capacitance, and V_1 and V_2 are the voltage levels before and after the piezomotor actuation, respectively. As seen in Figure 5.7, there is a transient voltage fluctuation in the storage capacitor voltage during actuation. To eliminate the effect of this fluctuation, V_2 is determined by extending the steady-state voltage waveform after actuation, to the time of actuation. Since the actuation takes place at every 4 seconds, the average piezomotor actuation power demand is calculated as 0.12 mW (row 3 of Table 5.1), which corresponds to only 3.6% of the 3.38 mW harvested power. This value validates the main motivation of the thesis: The piezomotor energy demand is very low so that the system is able to operate the piezomotor without considerably affecting the power balance. Moreover, the piezomotor retains its position without consuming any energy due to its self-locking feature, which increases device efficiency at constant ambient frequency. The majority of the piezomotor power demand comes from the driver of the piezomotor, which is developed by the manufacturer. Redesigning the driver with primary focus on power efficiency will reduce its power consumption.
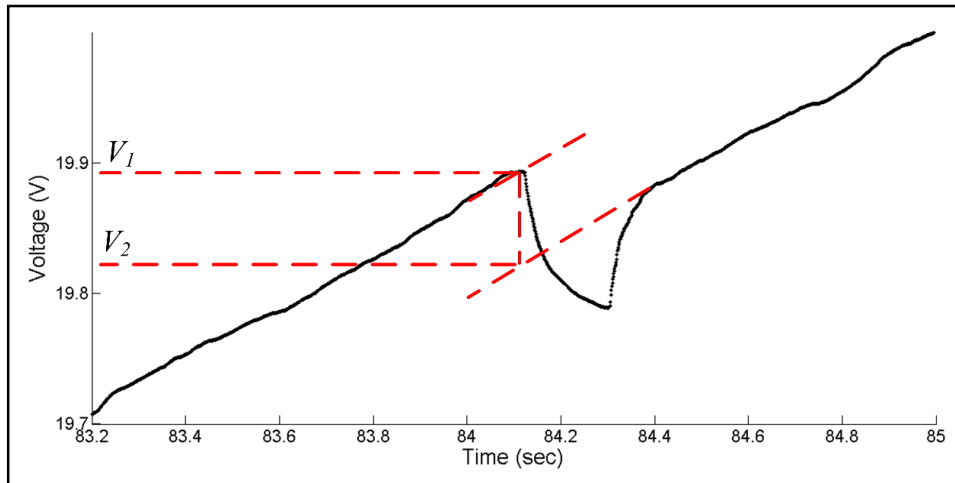
Figure 5.7. Storage capacitor voltage during piezomotor actuation. The effect of transient voltage fluctuation is eliminated by extending the steady-state voltage line and thus determining V2, the voltage after actuation

The harvested net power, i.e. the summation of the power supplied to the load and the power delivered to the storage capacitor is found to be 2.26 mW. This corresponds to 66.8% of the harvested power, which is a satisfactory result. Although minimizing the MCU and electronics power losses is not an aim of this research, it should be stated that these losses can be further reduced. A considerable part of them are due to the debugging purposed tasks of the MCU. For example, the MCU is awaked from sleep state frequently for monitoring certain parameters, which results in significant energy consumption. By optimizing the MCU tasks and decreasing its supply voltage, its energy consumption could be reduced to as low as 70 μW [23]. In this case, the efficiency will increase to as high as ~82%. In addition, using a storage capacitor with a higher capacitance will extend the duration of the system being able to perform the tuning algorithm smoothly, if the ambient vibration amplitude is too low.

5.4. MAXIMUM POWER CALCULATIONS

As it is mentioned at previous sections the optimum load gives the opportunity to harvest more electrical power from a piezo coupled beam. This is also true for the complete harvester. The previous power calculations are repeated with other voltage levels. The resulting curves are fitted to polynomials which includes the energy consumptions with

respect to the storage voltage. Therefore, net power generation difference is maximized at around 18.4 V, which indicates 4 mW of power generation of the piezo beams Figure 5.8.
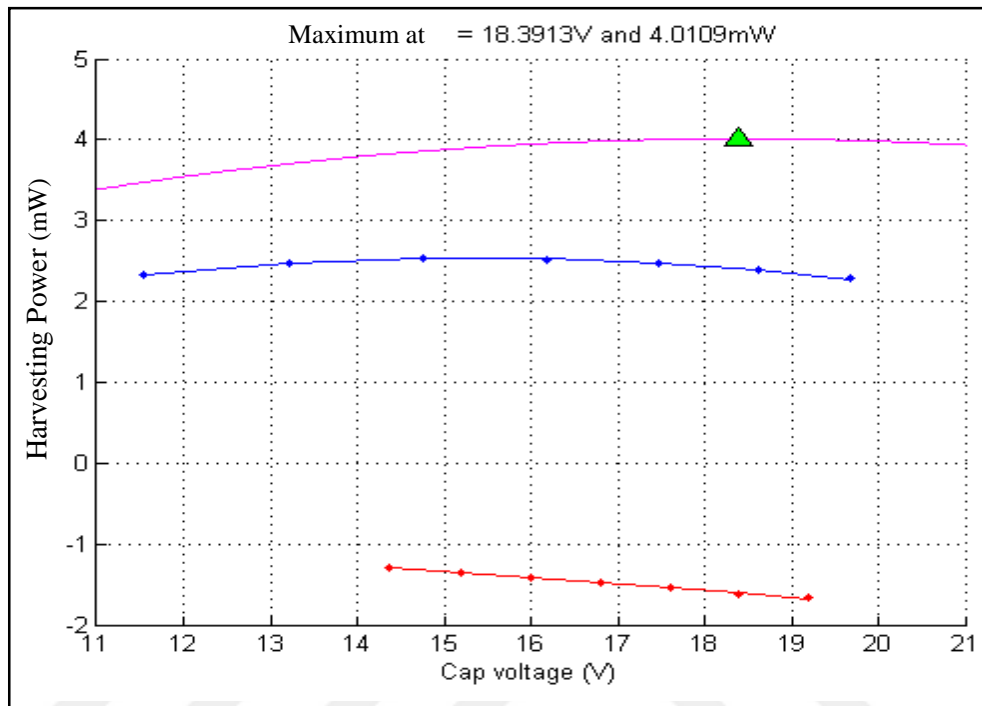

Figure 5.8. Power polynomials

6. CONCLUSIONS

A novel and efficient vibration energy harvester with self-sufficient natural frequency tuning mechanism is presented. The device is comprised of two off-the-shelf piezo-coupled beams, one of which includes a tip mass, movable by an actuator. The actuator used is a piezomotor, which is a miniature device with self-locking property. Self-locking property is very beneficial in minimizing the power losses at constant ambient vibration frequency. An algorithm that tunes the natural frequency based on the phase difference between the two beams is developed and successfully implemented in a low-power microcontroller unit. The system is able to self-adjust its natural frequency between around 49-54 Hz, which corresponds to a fractional bandwidth of ~10% whereas the fractional bandwidth of a not-tuned beam is ~4%. Increasing the piezomotor motion range will further improve the bandwidth. The tuning performance is unaffected by the nonlinearities of the system. The effect of period between frequency adjustments (sleep period) and rate of ambient frequency variation (sweep rate) on performance has been analyzed. It was shown that the algorithm is successful at a sweep rate of 1.03 Hz/min when the sleep period is 4 seconds. Increasing either the sweep rate or the sleep period results in tuning performance loss.

The harvester is able to simultaneously charge its storage capacitor, feed an external load and periodically actuate the piezomotor, at an ambient vibration of 1.05 gn at 53 Hz. This validates the self-sufficiency, since no external energy supply is used. A power distribution analysis revealed that at 53 Hz, the device can extract 66.8% of the harvested power into usable electrical power, even when the tip mass is forced to move at every 4 seconds. This value indicates that the device is able to perform frequency adjustment without requiring any external energy sources. The piezomotor power consumption corresponds to only 3.6% of total harvested power, which shows the success of using piezomotor for tuning. As for future work, we will concentrate on increasing the efficiency of power harvesting circuitry and the tuning algorithm implementation. We believe with improved power harvesting efficiency, the device will be a promising solution to wideband vibration energy harvesting problem in the near future.

REFERENCES

1. X. Dai, Y. Wen, P. Li, J. Yang and M. Li. Energy Harvesting from Mechanical Vibrations Using Multiple Magnetostrictive / Piezoelectric Composite Transducers. *Sensors and Actuators, A* 166:94-101, 2011.

2. S. P. Beeby, M. J. Tudor and N. M. White. Energy Harvesting Vibration Sources for Microsystem Applications. *Measurement Science and Technology,* 17:127-195, 2006.

3. D. Shen, J. H. Park, J. H. Noh, S. Y. Choe, S. H. Kim and I. H. C. Wikle. Micromachined PZT Cantilever Based on SOI Structure for Low Frequency Vibration Energy Harvesting. *Sensors and Actuators, A.* 154:103-108, 2009.

4. M. Marzencki, Y. Ammar and S. Basrour. Integrated Power Harvesting System Including a MEMS Generator and a Power Management Circuit. *Sensors and Actuators, A* 145-146:363-370, 2008.

5. B. A. Seddik, G. Despesse, S. Boisseau and E. Defay. Strategies for Wideband Mechanical Energy Harvester: Small-Scale Energy Harvesting. *Dr. Mickaël Lallart*, ISBN: 978-953-51-0826-9, InTech, 10.5772/51898, 2012.

6. M. Ferrari, V. Ferrari, M. Guizzetti, D. Marioli and A. Taroni. Piezoelectric Multifrequency Energy Converter for Power Harvesting in Autonomous Microsystems. *Sensors and Actuators, A* 142 329–335, 2008.

7. N. M. White, P. Glynne-Jones and S. P. Beeby. A Novel Thick-Film Piezoelectric Micro-Generator. *Smart Materials and Structures,* 10:850–852, 2001.

8. R. Ramlan, M. J. Brennan, B. R. Mace and I. Kovacic. Potential Benefits of a Non–Linear Stiffness in an Energy Harvesting Device. *Nonlinear Dynamics,* 59:545-558, 2010.

9. B. P. Mann and N. D. Sims. Energy Harvesting from the Nonlinear Oscillations of Magnetic Levitation. *Journal of Sound and Vibration,* 319:513-530, 2009.

10. M. F. Daqaq. Response of Uni-Modal Duffing-Type Harvesters to Random Forced Levitation. *Journal of Sound and Vibration,* 329:3621-3631, 2010.

11. A. Erturk and D. Inman. On Mechanical Modeling of Cantilevered Piezoelectric Vibration Energy Harvesters. *Journal Intelligent Material Systems and Structures,* 19:1311-1325, 2009.

12. C. Stanton, B. McGehee and B. Mann. Reversible Hysteresis for Broadband Magnetopiezoelastic Energy Harvesting. *Applied Physics Letters,* 95:174103, 2009.

13. C. Stanton, B. McGehee and B. Mann. Nonlinear Dynamics for Broadband Energy Harvesting: Investigation of a Bistable Piezoelectric Inertial Generator. *Physica D: Nonlinear Phenomena,* 239:640-653, 2010.

14. M. Ferrari, V. Ferrari, M. Guizzetti, B. Ando, S. Baglio and C. Trigona. Improved Energy Harvesting from Wideband Vibrations by Nonlinear Piezoelectric Converters. *Sensors and Actuators, A* 162:425-231, 2010.

15. Ö. Zorlu, E. Topal, and H. Kulah. Vibration-Based Electromagnetic Energy Harvester Using Mechanical Frequency Up-Conversion Method. *IEEE Sensors Journal*, 2011.

16. N. Topaloglu, A. A. Aksekili and B. Yegin. An Optimized Damping Model for Vibration Based Energy Harvesters with Constrained Proof Mass Motion. *IWPMA 2011 and the 6th Annual Energy Harvesting Workshop,* 2011.

17. M. O. Mansour, M. H. Arafa and S. M. Megahed. Resonator with Magnetically Adjustable Natural Frequency for Vibration Energy Harvesting. *Sensors and Actuators, A* 163:297-303, 2010.

18. S. Turkyilmaz, O. Zorlu, A. Muhtaroglu and H. Kulah. An Electromagnetic Micro-Power Generator for Low Frequency Vibrations with Tunable Resonance. *Procedia Engineering*, 25:729-732, 2011.

19. S. Huang and K. Lin. A Novel Design of a Map-Tuning Piezoelectric Vibration Energy Harvester. *Smart Materials and Structures,* 21:085014, 2012.

20. C. Eichhorn, R. Tchagsim, N. Wilhelm and P. A. Woias. Smart and Self-Sufficient Frequency Tunable Vibration Energy Harvester. *Journal of Micromechanics and Microengineering,* 21:104003, 2011.

21. Mide, "Mide Piezoelectric Energy Harvesters, VoltureTM rev. 001", http://www.mide.com/pdfs/Volture_Datasheet_001.pdf [retrieved 1 October 2010].

22. The PiezoWave®, "Product Datasheet: PiezoWave® Linear Motor 0.1 N", http://www.micromo.com/micromo/PiezoLinear/WAVE_LILINE_0.1_N_WL0104A_08A,08B.pdf [retrieved 5 November 2006].

23. Texas Instruments Incorporated, "MSP430G2x52 MSP430G2x12 Mixed Signal Microcontroller", http://www.ti.com/lit/ds/symlink/msp430g2252.pdf [retrieved 12 May 2013].

24. C. V. Karadag and N. Topaloglu. A Piezoelectric Cantilever Beam with Tunable Natural Frequency. *IWPMA 2013 and 8th Annual Energy Harvesting Workshop*, 2013.

25. Linear Technology, "LTC 3588-1 Nanopower Energy Harvesting Power Supply", http://cds.linear.com/docs/en/datasheet/35881fb.pdf, [retrieved 2 April 2010].

APPENDIX A: A BLIND-SEARCH BASED FREQUENCY TUNING

A blind-search based frequency tuning algorithm has been implemented earlier [24], that can be expressed as the following: The tip mass is first moved in an arbitrary direction and the required direction of motion that increases output power is determined, by checking the change in the voltage amplitude. In this way, practicing any motor actuation gives the information whether the resonance frequency of the beam is below the ambient frequency or above, and therefore the following direction of motor movement is supposed to tune the adjustable beam and increase power generation.

Any periodical update of the motor position may be a miss but at least one subsequent motor movement is observed as successive. This algorithm is tested under sweeping ambient frequency between two the resonance frequencies corresponding to the two limiting motor positions. The frequency responses of those positions are plotted on the same graph including the one that motor poisons are updated periodically rendering the blind search tuning algorithm, see Figure A.1.
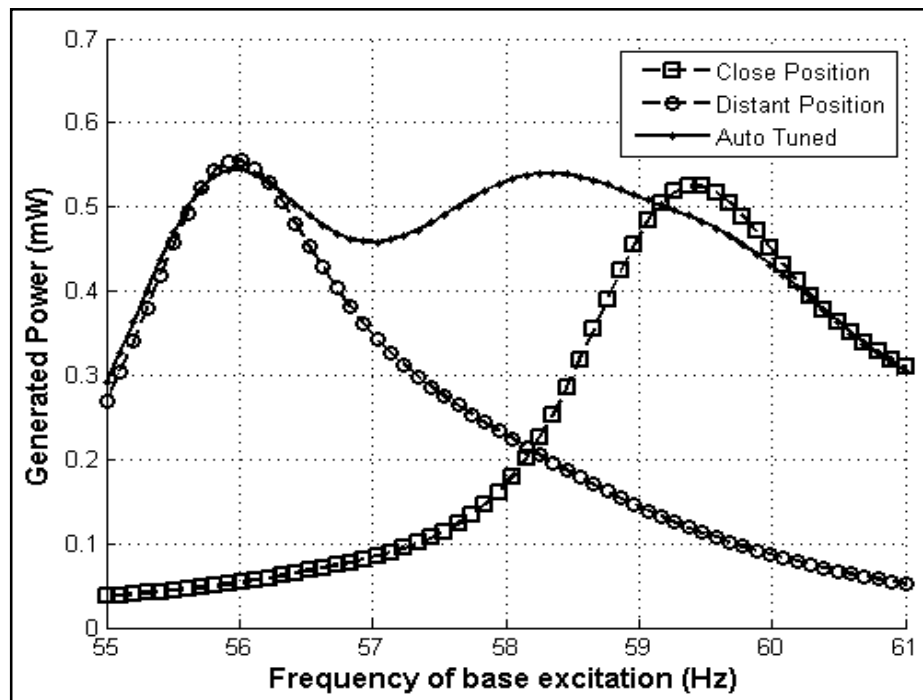

Figure A.1. The performance of the blind search algorithm

Under the steady frequency sweep rate, the frequency response of active tuning successively covers most of the effective energy generating regions on domain for the each individual fixed motor positions. Although this method requires virtually no sensor and it can keep the resonance condition, the movement of the tip mass can be very energy-consuming due to possible arbitrary movement directions, which contradicts the objective of being self-sufficient. Therefore, blind-search method is not preferred.

APPENDIX B: MEASUREMENT AND EVALUATION

Flowchart and explanations of measurement and evaluation of the data on the project in Figure B.1.
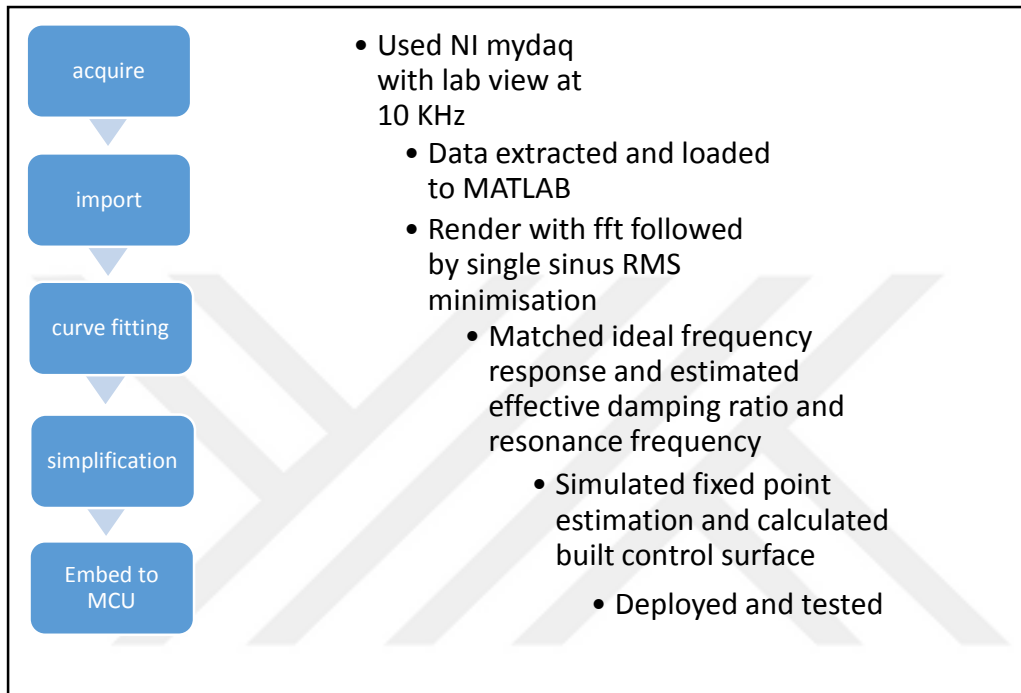
Figure B.1. Measurement and evaluation flowchart

APPENDIX C: CURVE FITTING OPERATION

Curve fitting operation which is explained in Appendix B that runs on custom written MATLAB script to fit second-order mass spring dampener system in Section 3.1 is applied on fixed beam shown in Figure C.1.
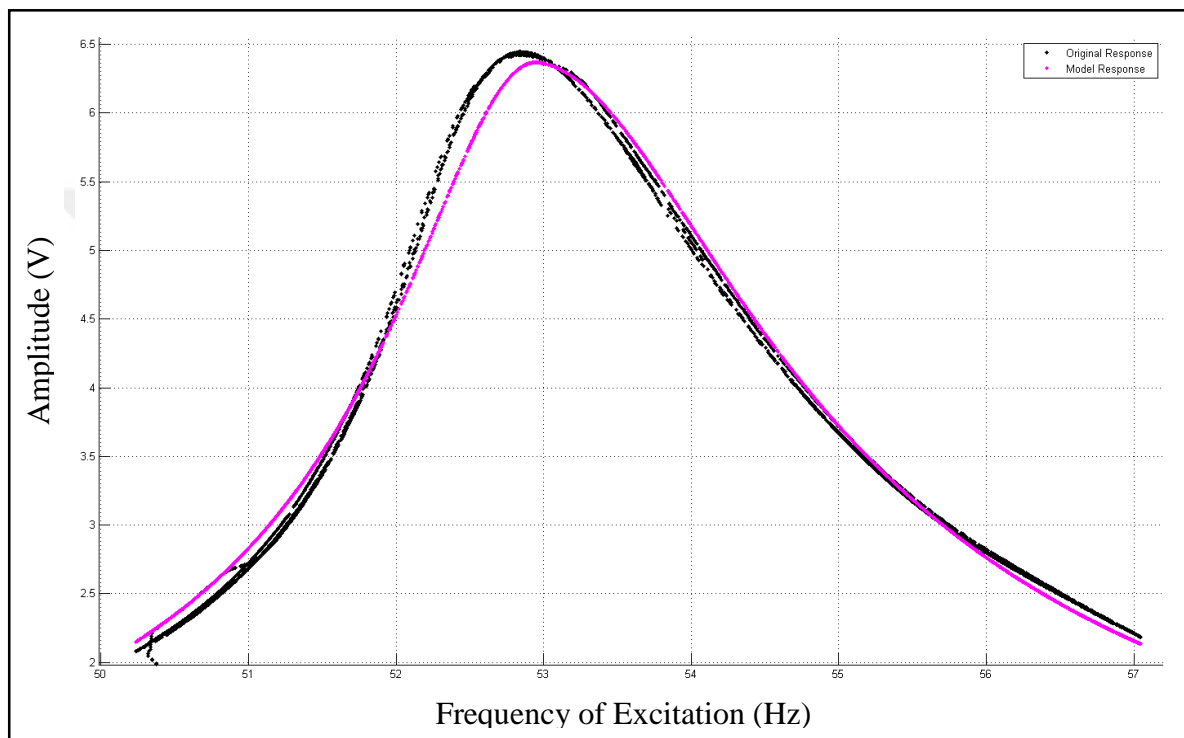

Figure C.1. Second order model fit for the frequency response of the beam

APPENDIX D: FRACTIONAL BANDWIDTH ESTIMATOR

Automated fractional bandwidth estimator calculates the maximum peak points per sweeps. Then the frequencies that are the projections where amplitude is $1/\sqrt{2}$ of the peak is matched. The match points are recorded for every sweep for every experiment result, see Figure D.1.
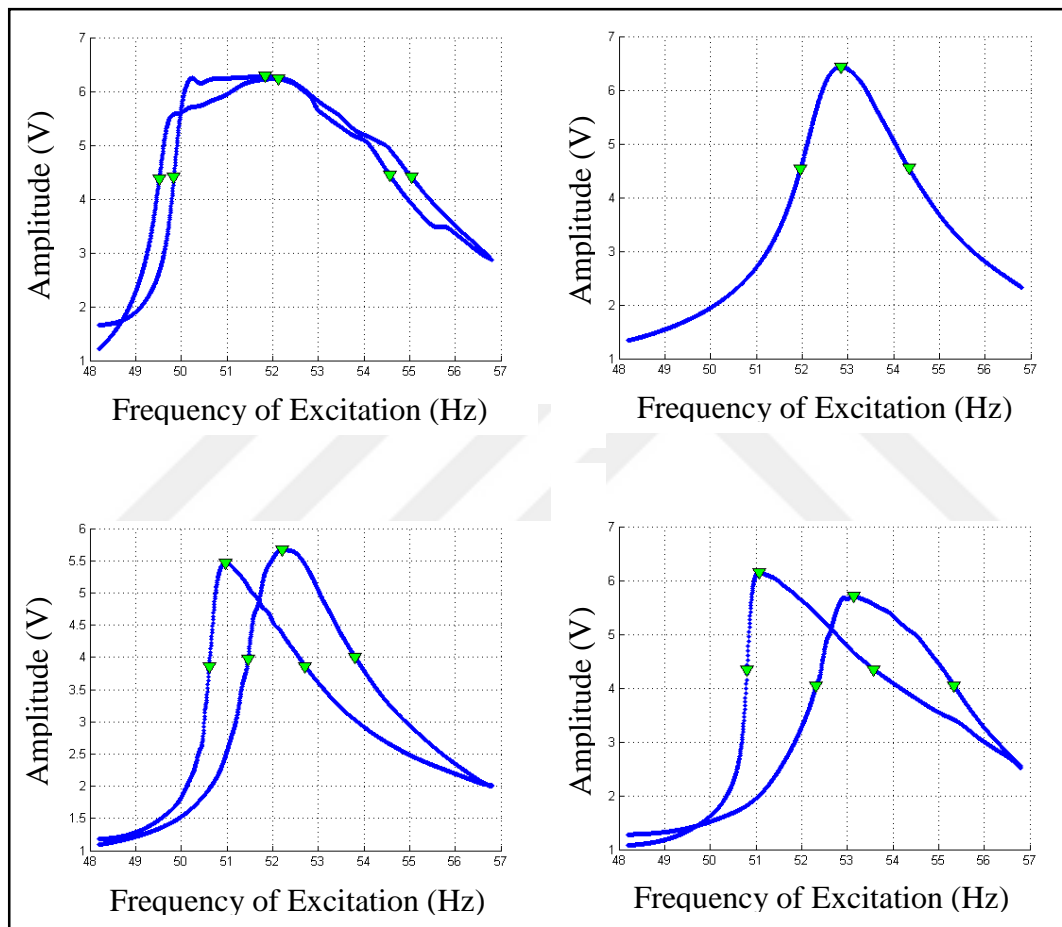

Figure D.1. Application of the fractional bandwidth method applied on experimental results

APPENDIX E: FREQUENCY COMPLEMENTARY FILTER

A custom MATLAB script is implemented for filtering operations. RMS filtered data and frequency complementary filtered Data are compared; in Figure E.1, RMS data has lesser fluctuation frequency while complementary filtered Data has lesser fluctuation shown in Figure E.2. Therefore, frequency complementary filter is used in all experimental analysis due to frequency analysis in the thesis.
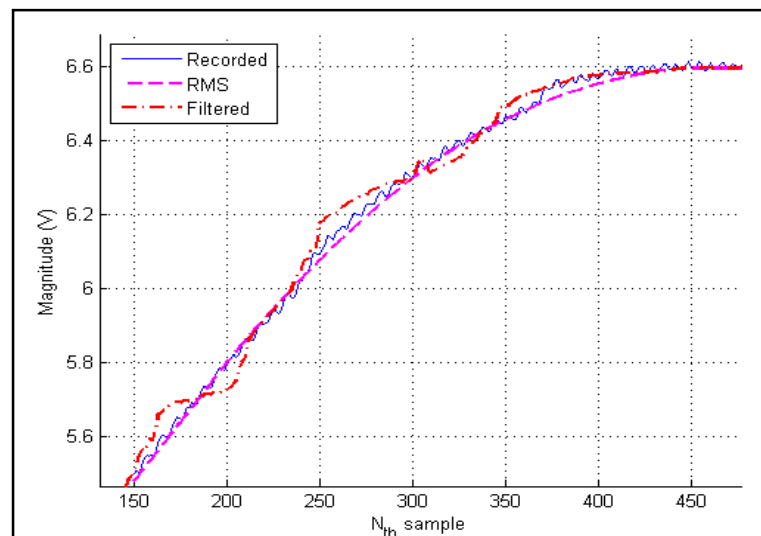
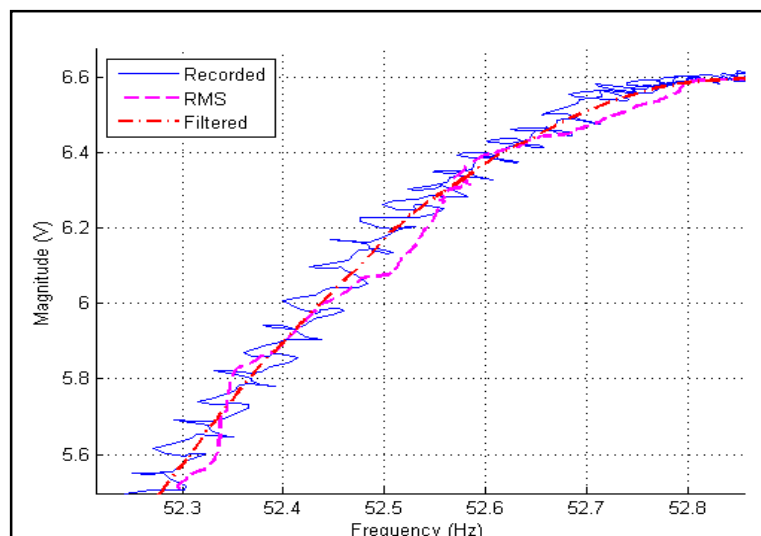

Figure E.1. Time Sampled Magnitude Data

Figure E.2. Frequency Sampled Magnitude Data

APPENDIX F: CAPACITOR VOLTAGE TESTS

In order to estimate power budget, the capacitor voltage tests which are explained in Section 5.3, are handled by segmenting recorded data in given timestamps. Every segment between timestamps are used to fit first order polynomials where those polynomials are used to estimate corresponding energy values. Picked capacitor consumption sub steps shown in Figure F.1, and energy harvesting sub steps shown in Figure F.2 in order to depict the procedure.
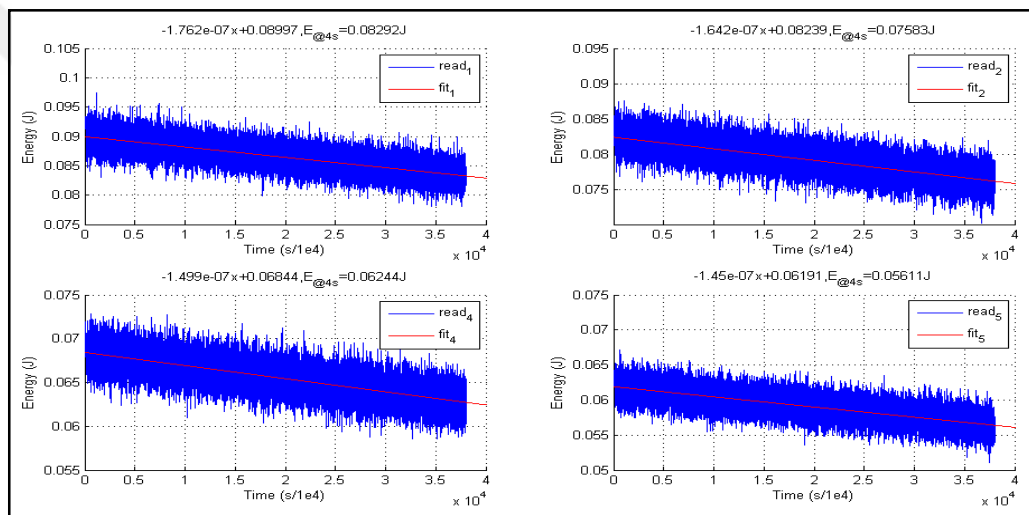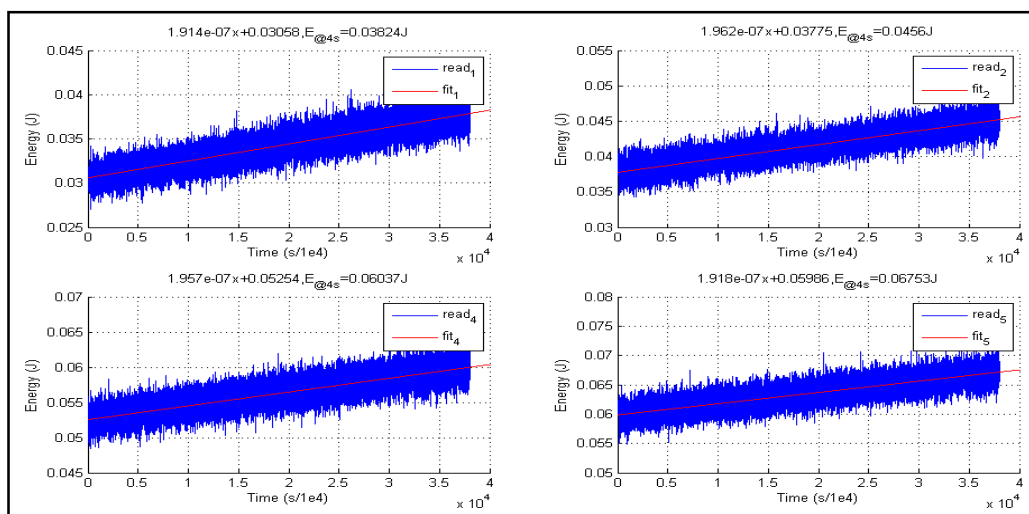

Figure F.1. Decreasing Order Power Analysis

Figure F.2. Increasing Order Power Analysis